Controls on cave drip water temperature and implications for speleothem-based paleoclimate reconstructions

Rau, Gabriel C.; Cuthbert, Mark O.; Andersen, Martin S.; Baker, Andy; Rutlidge, Helen; Markowska, Monika; Roshan, Hamid; Marjo, Christopher E.; Graham, Peter W.; Acworth, R. Ian

DOI:
10.1016/j.quascirev.2015.03.026

Controls on cave drip water temperature and implications for speleothem-based paleoclimate reconstructions

Gabriel C. Rau[*,1,2], Mark O. Cuthbert[2,3], Martin S. Andersen[1,2], Andy Baker[2], Helen Rutlidge[2,4], Monika Markowska[2,5], Hamid Roshan[1,2], Christopher E. Marjo[4], Peter W. Graham[2,6], R. Ian Acworth[1,2]

1. Connected Waters Initiative Research Centre, UNSW Australia, 110 King Street, Manly Vale, 2093, Australia
2. Connected Waters Initiative Research Centre, UNSW Australia, Sydney, NSW 2052, Australia
3. School of Geography, Earth and Environmental Sciences, University of Birmingham, Edgbaston, Birmingham, B15 2TT, UK
4. Mark Wainwright Analytical Centre, UNSW Australia, Sydney, NSW 2052, Australia
5. Australian Nuclear Science and Technology Organisation, Lucas Heights NSW 2234, Australia
6. SGA Environmental, Suite 8, 599 Pacific Highway, St Leonards, NSW 2065, Australia

* Corresponding author:

Gabriel C. Rau (gabriel.rau@unsw.edu.au)

UNSW Australia, 110 King Street, Manly Vale NSW 2093

Phone: +61 2 80719850, Fax: +61 2 9949 4188

KEYWORDS: Drip water temperature, speleology heat transport, paleoclimate archive, speleometeorology.

Invited to the thematic speleothem issue, "Novel approaches to and new insights from speleothem-based climate reconstructions", in *Quaternary Science Reviews.* Guest editors: Corinne I. Wong and Daniel O. Breecker (QSR Editor Claude Hillaire-Marcel)

Abstract

While several studies explore cave climate and thermal regimes, little is known about the controls on cave drip water temperature. Yet water temperature significantly influences biogeochemical processes associated with cave drips. To identify the processes that control the cave drip water temperature, we measured the temperatures at multiple locations along a speleothem flow path and drip sources (stalactites) concurrently with the drip rates in Cathedral Cave, Wellington, Australia. We monitored long-term drip water temperature, drip rates, surface and cave climate and in-cave evaporation rates and conducted 3 infiltration experiments with different flow, temperature and isotopic conditions. Our results show that the drip water temperature is controlled by multiple superimposed heat transport mechanisms that act upon the infiltrating water in the epikarst, the water film after it enters the cave and before it becomes a drip. The two main heat sources/sinks for drip water are the cave air and the surrounding rock. The subsurface temperature is coupled to the surface temperature by conduction through the soil and rock mass, but the cave climate is also coupled to the surface climate by venting. On a regional scale drip temperatures are mainly driven by the annual ground surface temperature signal but damped with depth and shifted in time compared to the surface. On a local scale, the drip water temperature can differ significantly from cave air and speleothem temperature due to the latent heat exchange of evaporation and localised water film convection. The main controls are ground surface temperature, subsurface depth, air density induced ventilation, distance from entry and drip rate. We present a conceptual model that explains drip water temperature signals and provide signal driven guidance on best type and location for speleothem sampling. We anticipate that our results will significantly improve the understanding of temperature-dependent paleoclimate signals from speleothem archives.

1. Introduction

1.1. Context and Aims

Surprisingly little work has been done on what controls the temperature of cave drip water and yet this is of fundamental importance as it controls biogeochemical processes in caves. For example, drip water temperature influences the growth rate of speleothems [Dreybrodt, 1981; Baker et al., 1998], fractionation of isotopes [Epstein et al., 1953], and deposition of biomarkers [Schouten et al., 2007]. In speleometeorology, latent heat exchange processes such as condensation or evaporation alter the thermal energy content of drip water [De Freitas and Schmekal, 2003] and can lead to cooling of speleothems [Cuthbert et al., 2014a]. Finally, in geomicrobiology, the habitat of cave microorganisms is strongly influenced by temperature [Northup and Lavoie, 2010].

Cave drip water originates from precipitation or surface flow, which infiltrates the soil surface. It is well recognised that the dynamic temperatures at the earth's surface propagate into the subsurface [Stallman, 1965; Baker and Ruschy, 1993]. Near-surface temperature measurements can be used to quantify water flow [Rau et al., 2014], for example by exploiting temperature-time variations [Taniguchi and Sharma, 1993; Bendjoudi et al., 2005] or temperature depth profiles [Tabbagh et al., 1999; Cheviron et al., 2005]. Fluctuating ground surface temperatures are damped with depth until a stable temperature is reached [Taniguchi, 1993; Smerdon et al., 2003]. The dominant mechanism of subsurface heat transfer beyond the soil zone is by conduction [Smerdon et al., 2003]. However, the influence of rock, as opposed to air, temperature profiles on cave drip water temperature has not been investigated.

Water commonly flows over speleothem surfaces such as flowstones, stalactites and draperies inside caves before arriving at the drip source (falling films) [i.e., Camporeale and Ridolfi, 2012]. During film flow a number of different heat and mass transfer mechanisms act simultaneously. While the engineering literature reports on simultaneous heat and mass transfer during film flow [i.e., Yan and Soong, 1995], cave related sciences have not investigated the effects of film flow heat transport on the cave drip water temperature. Yet it is well accepted that water films will exchange moisture and heat with the cave air [Atkinson et al., 1983; Faimon et al., 2012].

Cave water is generally in contact with cave air for some time before forming drips. Cave climate must therefore be considered when investigating what controls cave drip water temperatures for caves that are open to the atmosphere. It has been shown that surface air

temperature anomalies can affect cave air temperature [Dominguez-Villar et al., 2013, 2014]. A change in cave climate is associated with advective air flow by venting [De Freitas et al., 1982; De Freitas and Littlejohn, 1987]. Cave venting is caused by barometric pressure changes, density differences between cave and surface air (chimney effect) [Conn, 1966; Wigley, 1967; Oh and Kim, 2011] or through winds across the entrances (venturi effect) [Kowalczk and Froelich, 2010]. Cave-atmosphere air exchange results in spatiotemporal variability of otherwise stable cave air temperature [Smithson, 1991; Perrier et al., 2010]. In a comprehensive investigation of cave air venting Faimon et al. [2012] determined the key drivers of the microclimatic variability.

The cave climate also responds rapidly but predictably to changing atmospheric climate conditions [Atkinson et al., 1983; De Freitas and Littlejohn, 1987]. Air flow can cause significant loss of water due to evaporation from caves [McLean, 1971] with increasing moisture loss for only small decreases in cave relative humidity below the saturation point [Buecher, 1999]. Cuthbert et al. [2014a] reported significant cooling of speleothems, and drip water, through in-cave evaporation.

Conversely, cave condensation and its change to the overall thermal energy balance were also found to relate to cave air temperatures [De Freitas and Schmekal, 2003]. Condensation can increase the temperature of cave walls [Dreybrodt et al., 2005]. Further, considerable speleothem dissolution can be caused by condensation through the formation of calcite undersaturated drips [Rozemarijn et al., 1998]. Importantly, cave climate exerts significant control on speleothem deposition through the temperature dependence of both kinetic and equilibrium drip water geochemical processes [Spötl et al., 2005; Baldini et al., 2008]. However, the in-cave climatic controls on cave drip water temperature have also yet to be explored systematically.

When considering temperature as a control for water related cave processes and the interpretation of temperature-dependent speleothem paleoclimate proxies, the cave air temperature is generally used, since it is easily measured. Here, we illustrate that the true cave drip water temperature can differ significantly from cave air temperature and we identify the processes exerting control. Hence the aim of this paper is to identify and describe the controls on cave drip water temperature. We systematically investigate the dominant influences on cave thermal regimes and drip water temperature by analysing subsurface heat (and mass) transport through the karst and the atmospheric connection. Examples for the different controls are presented using measurements of drip rate, speleothem and drip water

temperature as well as climate data monitored inside the cave and on the land surface. Using this data we demonstrate how a surface air temperature climate signal will be propagated to a cave, and how the resulting drip water temperatures may deviate from the mean annual air temperature.

1.2. Description of the field site and prior work

Data presented in this paper was acquired at Cathedral Cave in the Wellington Caves Reserve (Latitude -32.622°, Longitude 148.940°) in New South Wales, Australia. Figure 1 shows the location and horizontal dimensions of Cathedral Cave. Cathedral Cave is located in a temperate semi-arid zone. The Caves Reserve is exposed to a significant seasonal variation in the surface air temperature between approx. 0 to 45 °C, with a mean annual maximum temperature of 24.3 °C. Long-term annual average rainfall in the area is episodic with approx. 617 mm/year, and the relative humidity varies between 6-98 % with a mean annual value of 68 % [BOM, 2014].

The cave system is located in the Molong Anticlinorial Zone and intersects a massive and thinly bedded Devonian limestone [Osborne, 2007]. Cathedral Cave is one of the larger caves featuring two nearby entrances and has a vertical depth of approx. 25 m. As a show cave it is well-developed with infrastructure suitable for tourist groups. The cave is easily accessible and offers an ideal opportunity to investigate subsurface karst processes, such as karst hydrology, geochemistry and paleoclimate signals in speleothems. The cave has been subject to long-term drip rate and drip water monitoring starting in 2009 and ongoing. Jex et al. [2012] correlated spatially distributed drip records and found that they group into distinct categories of differently behaving clusters indicative of the flow path features. Mariethoz et al. [2012] identified chaos in drip rates and concluded that this contains information about flow routing in fractured media. Rutlidge et al. [2014] found clear soil and limestone signatures in the drip water through trace elements and organic matter analysis. Cuthbert et al. [2014b] reported that cave drip water is only activated after long duration and high volume rainfall, and that evaporation from the epikarst is an important control on drip water isotopic composition.

2. Materials and methods

2.1. Surface irrigation

Owing to the temperate semi-arid climate at the Wellington Caves Reserve, rainfall events sufficient to overcome the soil moisture deficit and trigger cave dripping are erratic [Jex et al., 2012; Mariethoz et al., 2012]. To induce dripping in the shallow cave so that controls on cave drip water temperature could be investigated a total of 3 controlled surface irrigation experiments were conducted over a two-year period (2013-2014). Geochemical results of the first irrigation experiment were previously published in Rutlidge et al. [2014] and drip water temperature data from the second irrigation experiment has been reported in Cuthbert et al. [2014a].

During the surface irrigations a patch size of ~24 m^2 (2013) and ~50 m^2 (2014) above the near-surface chamber of Cathedral Cave (see Figure 1) was hand hosed with town water from a storage tank. Two summer and one winter irrigation campaigns were conducted. The dates and specifics of each of the three surface irrigation experiments are summarised in Table 1. Importantly, during the first irrigation experiment, the temperature of first and third continuous surface application was set to approx. 0.3 ºC using ice bags. Further, deuterium was added as a conservative tracer to the batch of water first applied (enrichment of ~6100 ‰ VSMOW) during surface irrigation in 2013. Markowska et al. [submitted] provide a detailed analysis of the deuterium tracer measured during the same experiments as well as long-term monitoring of natural isotopic composition.

2.2. Cave and surface monitoring

Different sites were selected for monitoring at increasing cave depths and distance from cave entrance (Figure 1). To measure the drip water temperature we affixed automated miniature temperature loggers (DST micro T, StarOddi, Iceland) along known flow paths of water on top of the speleothem (flowstone), with a logger mounted to the tip of the drip source (stalactite, Figure 2B). The loggers were selected based on their small size, rapid temperature response time (~20 s), resolution (0.01 ºC) and accuracy (±0.2 ºC). These features make the loggers an ideal choice for monitoring drip water temperature. The cave air temperature was also measured in close proximity to the drip source (Figure 2A). During the irrigation experiment in January 2013 (southern hemisphere summer) the shallow soil temperature of the irrigation patch was monitored at 2 locations with DST micro T loggers (Figure 1).

In the January 2014 irrigations, in addition to the StarOddi loggers, detailed temperature measurements were acquired with high accuracy (±0.002 ºC) and resolution (0.0006 ºC)

custom-build instrumentation. The sensors consisted of Platinum resistors (Pt1000, 1 kΩ at 0 ºC) embedded in flat aluminium housing (25 x 6 x 1 mm – see Figure 2C) designed for fast thermal response. Figure 2 shows sensors deployed along a flow stone and stalactite near the entry (site A, location in Figure 1). More details about method and results from this deployment are reported in Cuthbert et al. [2014a]. Here, we use a subset of this data for a more detailed and comprehensive description of the heat transport processes that exert control on cave drip water temperatures.

The drip locations were also monitored continuously with automated drip counters (Stalagmate, Driptych, UK). Further, climate monitoring stations consisting of relative humidity and temperature sensors (HMP155A, Campbell Scientific, USA) were deployed at 2 different locations to record the cave air. Cave barometric pressure was also measured using a pressure transducer (Levellogger, Solinst Inc., Canada). Water samples were regularly collected from drip sources at site A with 20 ml glass McCartney bottles. The samples were analysed using a Los Gatos® cavity ring down laser spectrometer with overall precision of ±2.0‰ δ^2H. Evaporation pans (9.5 cm inner diameter) were deployed at site A and C (Figure 1) for extended periods of time. Volumetric water loss was measured using a digital pipette, precision scale and the pan size, and the evaporation rate was calculated from the time of pan deployment.

Surface climate variables, i.e. air temperature, shallow soil temperature and moisture, relative humidity and barometric pressure, were monitored by a climate station (Hill Climate Station, Wellington, data download available: http://groundwater.anu.edu.au/) located in close proximity south-east of Cathedral Cave. Precipitation data was recorded by a rain gauge in Wellington ~6.5 km away (Agrowplow, station 065034) [BOM, 2014]. The thickness of the soil zone was found to vary from 0 to 0.5 m estimated by inserting a thin metal rod into the soil across the irrigation patch. During the 2014 experiment volumetric soil moisture integrated across the upper 10 cm was measured frequently at random spots across the irrigation patch with a handheld meter (MPM160, ICT International, Australia).

2.3. Data processing

2.3.1. Surface to subsurface heat conduction

The Earth's surface is exposed to time variable heat influx from solar radiation, which forms a significant energy source for subsurface propagation. The periodicity of insolation is controlled through the earth and solar cycles. Hence, surface air temperature contains distinct frequencies, i.e. daily, annual, decadal, centennial, millennial, as well as aperiodic

environmental influences related to local weather and climate, i.e. high and low pressure systems, and oscillation indices. Cave temperatures have been related to ground surface and surface air temperatures by analysing heat propagation with depth through conduction assuming that thermal properties can be depth averaged [Smerdon et al., 2003, 2004].

Carslaw and Jaeger [1959] formulated a 1D differential heat conduction equation. The equation was solved with a harmonic temperature boundary at the top and a constant temperature boundary at infinite depth. This resembles the subsurface environment between surface and cave. Since the heat transport equation is of linear nature, the analytical solution is valid for any harmonic component of temperature variation with an individual frequency (e.g. daily or annual) that is part of the total temperature signal [Goto et al., 2005].

Here, we consider that thermal diffusivity for soil can vary due to differences in saturation [Ochsner et al., 2001], compared to low porosity bedrock which can be assumed to be constant over time. Consequently, it is useful to separate the subsurface into two layers: soil zone and epikarst zone. While several studies have used shallow multi-level soil temperature measurements to calculate near-surface infiltration [Smerdon et al., 2004; Bendjoudi et al., 2005; Cheviron et al., 2005] the propagation of thermal waves into rock above the groundwater table is predominantly controlled by thermal diffusion [Smerdon et al., 2003].

To calculate the dynamic subsurface rock temperature through two layers, an analytical solution [Carslaw and Jaeger, 1959; Goto et al., 2005] is modified as

$$\mathrm{T}_i\left(\mathrm{z},\mathrm{t}\right) = T_0 + \mathrm{A}_i \cdot \exp\left(-\sqrt{\frac{\pi}{\mathrm{P}_i}}\left(\frac{\mathrm{d}_s}{\sqrt{D_s}} + \frac{z-\mathrm{d}_s}{\sqrt{D_r}}\right)\right) \cdot \cos\left(2\pi\frac{\mathrm{t}}{\mathrm{P}_i} - \sqrt{\frac{\pi}{\mathrm{P}_i}}\left(\frac{\mathrm{d}_s}{\sqrt{D_s}} + \frac{z-\mathrm{d}_s}{\sqrt{D_r}}\right) - \theta_i\right) \quad (1)$$

for $z \geq d_s$. Here, i is a distinct harmonic temperature component with period P_i [d]. T_i is the temperature [°C] due to harmonic temperature component i as a function of depth z below subsurface [m] and t is time [d]; T_0 is the mean surface temperature [°C]; A_i is the amplitude [°C] of the harmonic signal i; θ_i is a phase offset [rad]; d_s is the thickness of the soil layer [m].

In Equation 1, D is the effective thermal diffusivity for the soil layer (subscript s) and the epikarst (subscript r). In general, the thermal diffusivity [m^2/d] is defined as [Carslaw and Jaeger, 1959]

242 (2) $$D = \frac{\kappa}{\rho c}$$

243 where κ is the bulk thermal conductivity [W/m/K] for variably saturated soil or solid rock [de
244 Vries, 1963; Tarnawski, 2011; Horai, 1971; Clauser and Huenges, 1995]. Analogously, the
245 bulk volumetric heat capacity ρc [MJ/m^3/K] is reported for sediments and rock [Schön, 1996;
246 Schärli and Rybach, 2001].

247 Equation 1 can be used to predict the subsurface temperature response to a particular
248 frequency component of interest extracted from the ground surface temperature data. For
249 example the i-th component could be daily, annual, centennial, millennial, or any other
250 significant component determined using a Fourier transform analysis of dominant
251 frequencies. In Equation 1 the exponential part accounts for temperature amplitude damping
252 and the cosine part for the shift in phase over depth. The phase offset θ is the time relative to
253 the maximum insolation (summer solstice on 21 December in the southern hemisphere) and
254 accounts for any difference between the conduction theory and realistic conditions.

255 In this paper we use 2 different layers, one representing the soil and one the limestone. We
256 measured the thermal conductivity and heat capacity of soil and limestone samples collected
257 at the Cathedral Cave field site (Figure 1) using a KD2 Pro thermal analyser (Decagon
258 Devices, US). To account for the variable water saturation of the soil (i.e. dry and saturated
259 end members), the soil parameters were measured after oven drying (105 °C, 6 hours) and
260 after saturating the soil sample with water. Further, a piece of limestone bedrock had holes
261 drilled for inserting the instrument needles, and a highly conductive paste was used to ensure
262 optimal thermal bridging between needle and limestone sample. The measured thermal
263 parameters are listed in Table 2.

264 Equations 1 & 2 were used to simulate the annual temperature variations (with $P = 365.25$ d)
265 at various depths of interest. Models were fitted to temperature observations by varying
266 parameters as outlined in Table 4 and minimising the normalised root mean square error
267 (NRMSE). For the surface air temperature the parameters of interest were mean annual
268 temperature (T_0), amplitude (A) and phase offset from solstice (θ) while the depth was set
269 to zero ($z = 0$). For the cave air and flowstone temperatures the parameters of interest were
270 mean annual temperature (T_0), depth of limestone (z) and phase offset (θ). Here, the
271 remaining parameters were set as follows: Amplitude A as determined from the surface air

272 temperature fit, soil zone thickness $d = 0.1$ m, thermal diffusivities as measured on soil and a
273 limestone sample (Table 2).

274 **2.3.2. Air density calculation**

275 A well-known process of cave atmosphere air and moisture exchange is venting stimulated
276 by the difference in density between atmospheric and cave air (the chimney effect) [Conn,
277 1966; Wigley, 1967; Oh and Kim, 2011]. The density of air can be calculated taking into
278 account thermodynamic properties of dry air as well as water vapour [Giacomo, 1982]. It is
279 expressed as

280 (3) $$\rho_a = \frac{pM_a}{ZRT}\left[1 - x_v\left(1 - \frac{M_v}{M_a}\right)\right]$$

281 where p is the barometric pressure [Pa]; Z is the compressibility coefficient, under the
282 conditions reported here of value 0.999611566 [-]; R is the universal gas constant, 8.31441
283 [J/K/mol] and T is the temperature [K]; M_a and M_v are the molar mass of dry air
284 0.0289635 [kg/mol] and water vapour 0.018015 [kg/mol]. The mole fraction of water vapour
285 in moist air x_v is defined as

286 (4) $$x_v = \frac{h}{p} exp\left(AT^2 + BT + C + DT^{-1}\right) f$$

287 where h is the relative humidity $(0 < h < 1)$; f is an enhancement factor, under the
288 conditions reported here of value 1.0038 [-]; the saturation vapour pressure coefficients are
289 published as $A = 1.2811805 \cdot 10^{-5}$ [K^{-2}], $B = -1.9509874 \cdot 10^{-2}$ [K^{-1}], $C = 34.04926034$,
290 $D = -6.3536311 \cdot 10^{3}$ [K]. For above parameter values please refer to Giacomo [1982].

291 Equations 3 and 4 require measurement of the common variables that define the
292 thermodynamic state of moist air: barometric pressure, air temperature and relative humidity
293 (RH). To investigate cave venting, air densities were calculated from the surface and cave
294 climate records for a 2-week period during both summer and winter in 2014.

3. Results

3.1. Surface and cave climate

Figure 3 shows surface air temperature and rainfall recorded at the surface above Cathedral Cave over a 2-year period between 2012 and 2014. Cave air temperature measured near site A is also shown. A climatic summary for the period between Jan 2013 and Dec 2014 is as follows: The minimum and maximum surface air temperatures were -2.9 °C and 43.5 °C. Typical for a temperate semi-arid climate, relative humidity varied between 5-98 %, with a median of ~63 %. For more than half of the year (233 d) the volumetric soil moisture content was below the median annual value of 21 % because evapotranspiration generally exceeds precipitation.

While ~312 days/year were without significant rain (< 1 mm/day), below average yearly total of 550 mm was recorded from episodic rainfall events occurring on 86 days/year. On 1 March 2013 a maximum daily rainfall of 74 mm was recorded. The amount of rain from this natural event was comparable to the manual application of water on the irrigation patch during the surface irrigation experiments (Table 1 and Figure 1).

At Site C, the air and speleothem temperature was very stable at 17.8 ºC with only minor fluctuations of ~0.1 ºC between January-December 2014. Cave relative humidity (RH) was measured at 10 min intervals during parts of the year between January and November 2014. The RH, recorded at site A, fluctuated significantly with minimum, maximum and median values of 59.3 %, 97.9 % and 88.6 %, respectively. At site C the RH showed very minimal fluctuations around a median value of 97.1 %, with minimum and maximum RH of 96.5 % and 97.8 %, respectively. Evaporation rates as measured at the different locations (Figure 1) during summer and winter 2014 are shown in Table 3. There is a clearly decreasing trend in evaporation rate with increasing distance from entrance in summer, with RH values increasing as expected. Noteworthy, however, is the stable but below saturation RH level at site C leading to some potential for evaporation from the deepest part of the cave throughout the year.

3.2. Drip water temperatures during irrigation experiments

Figure 4 presents high resolution temperature measurements, drip counts and relative humidity measured during irrigation experiment 2 conducted in January 2014 (summer). While the majority of the measurements in Figure 4 were previously published by Cuthbert et al. [2014a], we use this dataset as a starting point and present new results that reveal a detailed analysis of the different controls on cave drip water temperature.

Before the first surface irrigation the soil moisture across the irrigation patch was between 4-24 % indicating a high soil moisture deficit. Approx. 3 h after the start of the water application (~68 mm rainfall equivalent) the drip source responded with a rapid increase to approx. 140 drips/min (Figure 4B). Before the second irrigation the soil moisture was much higher with measurements ranging between 20 % and 37 %. After applying less water in the second irrigation (equivalent of ~48 mm rain) the drip source responded much quicker (~1 h after start) and showed significantly faster drip frequency (~180 drips/min) and longer drip activity compared to the previous day (Figure 4B).

Before the onset of dripping, temperature measurements taken on the dry speleothem surface along the expected drip water flow path (Fig. 2a) were relatively constant in time but with decreasing temperature from cave ceiling to drip source (stalactite) revealing a downward gradient approx. -0.8 °C/m (Figure 4A). Measured air temperatures reflect a spatial gradient that was similar to the one measured on the rock surface. Relative humidity measurements (RH) varied between a minimum of 79 % and a maximum of 91.5 %. A spot measurement near the chamber ceiling revealed RH of up to 98 % after the flowstone had been wet at the end of the irrigation experiment in Jan 2014.

Temperatures, measured after activation of cave dripping, exhibit a rapidly increasing temperature on all sensors, peaking at approx. ~0.3-0.8 °C above the original measurement coinciding with a peak at the maximum drip count (Figure 4A). This is followed by a slow temperature decrease as the drip rate decreases. At ~ 20 drips/min, the drip water temperatures measured by the lower sensors returned to the level measured before the onset of flow.

After a period of relatively stable measurements, the drip water temperature started to decrease, with lower sensors showing a more rapid and pronounced cooling of up to 1.5 ºC below the cave air temperature which was measured in close proximity. The onset of

observable evaporative cooling was at a RH of 90 %, and the increase in drip water cooling coincided with a rapid drop of RH to 79 %.

After the second surface irrigation the same temperature increases were observed but with stronger magnitude and longer duration, despite the application of less water at the surface. However, evaporative cooling was less pronounced reflecting the higher levels of RH (85-90 %) during this event compared to the first event.

Figure 5 summarises temperature and deuterium data as well as drip counts measured during irrigation experiment 1 conducted in January 2013. Note that the experimental procedure and measurement setup differed compared to experiment 2 described in the last section. Here, drip water temperature was only measured at the drip source (same stalactite as above). However, in addition shallow soil temperatures (~5 cm and ~10 cm below the surface) were measured, but cave air RH was not. It is noteworthy that 4 individual irrigations were applied (35-63 mm rainfall equivalent) and with the water during the first 3 applications cooled to ~0 °C, ~10 °C and ~0 °C, respectively.

Cave air temperature was relatively stable at approx. 17.5 ºC (Figure 5A), while the daytime outside air temperature peaked at approx. 40 ºC. During the time of experimentation the cave air temperature shows slight increases during the times at which the surface air temperature was at its lowest (night time). This excludes one occasion on 10 January 2013 where the cave air and drip water temperatures both decreased coincident with the surface air temperature falling below the average cave temperature (grey arrow in Figure 5B). Also noteworthy here is the response of the soil temperatures to the cooled irrigation water, with both sensors showing measurements as low as 5 ºC and 14 ºC which are clearly below the minimum surface air temperature of 15 ºC during that time (Figure 5A).

Drip water temperatures responded similarly to the surface irrigation during the January 2013 experiment (Figure 5D) compared to the experiment in 2014 (Figure 4B). Interestingly, the drip water temperature at the first drip activation with an average drip response of 80 drips/min shows a cooling event during which there was a significant temperature difference of -2.5 ºC between drip water and air temperature (Figure 5B). This was the response to an irrigation application where the water was cooled to 10 ºC, less than during the first irrigation (Figure 5A). A similar sized evaporative cooling event can be seen again during the drip recession caused by the last surface irrigation where ~24 ºC water was applied without the addition of ice. A clear deuterium enrichment (deuterium breakthrough) was measured in drip

385 water samples after the third surface application originating from the deuterium that was
386 added to the first irrigation batch (Figure 5C).

387 Drip water temperature after the third surface irrigation during which water was cooled again
388 to 0 °C showed a very small decrease before warming and tracking close to the cave air
389 temperature (Figure 5B). As soon as the drip rate fell below ~30 drips/min another
390 evaporative cooling event was observed. This time, however, it was overwhelmed by the last
391 surface application of water which carried warm water as film flow along the speleothem
392 surface.

393 **3.3. Long term air, speleothem and drip water temperature records**

394 Figure 6 shows the temperature data measured on the speleothem surface (dry or wet cave
395 over speleothem surfaces) at three different locations along the drip water flow path at site A
396 (see Figure 2) including the drip source (stalactite), air temperature and drip rate over a time
397 period of ~11 months. Figure 6 includes the response to surface irrigation experiment 3 (also
398 highlighted in Figure 3). The trend in all temperature data complies with a distinct annual
399 harmonic but with different amplitude and phase compared to surface air temperature. This
400 originates from subsurface conduction of the annual surface temperature wave, and we will
401 refer to this as the "background temperature".

402 Results from fitting surface air, cave air, speleothem and drip water temperature time-series
403 to Equation 1 with an annual periodicity are presented in Table 4 ordered by increasing total
404 depth. The best fitting annual harmonics are also plotted in Figures 3 and 6. Noteworthy here
405 is the characteristic amplitude damping and phase shifting with increasing total depth. While
406 the surface air temperature is offset from summer solstice by 20 days, there is a relatively
407 constant phase offset of ~11 to 12 days (compared to the surface air temperature) once the
408 annual temperature harmonic propagated through the subsurface. This indicates compliance
409 with the subsurface heat conduction theory (Equation 1). Further, total depths obtained from
410 the fitting procedure are in good agreement with the vertical cave dimensions estimated from
411 an in-cave survey (Figure 2A).

412 The two upper measurement points show relatively stable temperature over time, when
413 considering faster than annual frequencies, but with occasional upward and downward spikes
414 indicating fast advective film flow in summer and winter, respectively. However, the
415 temperature measured in air and the tip of the stalactite (Figure 2) shows marked fluctuations
416 with a daily frequency and varying amplitude of up to ~1 °C superimposed on irregular lower

417 frequency variations and the background temperature. A number of drip events with varying
418 magnitude and with a maximum of ~25 drips/min were recorded (Figure 6). At this point a
419 question arises: What causes the faster than annual temperature fluctuations?

420 **3.4. Examples of venting induced drip temperature changes**

421 Figure 7 shows a detailed snapshot of cave flowstone, 2 stalactites, and cave air temperature
422 (A, D) as well as cave RH (B, E), and surface and cave air density calculated using Equations
423 3-4 (C, F) during summer and winter in the year 2014.

424 In summer (Figure 7A-C), a small drip event triggered an upwards temperature spike ~0.5 °C
425 on the stalactite, followed by multiple cooling fluctuations with magnitude ~1.5 ºC
426 coinciding with rapid decreases in cave air RH due to the venting events. A decrease in cave
427 air temperature, with some delay, as a result of evaporative cooling, is also evident from the
428 data. The cooling events are similar to those observable during the irrigation experiments
429 (Figures 4A and 5A) but seem to occur with a daily frequency over certain periods (Figure 6).
430 When comparing this with the surface and cave air densities it is clear that the regular RH
431 decreases correlate well with periods where the surface air is denser than the cave air (note
432 that dry air is denser than humid air of the same temperature) in the early mornings causing
433 frequent cave venting events. Interestingly, evaporative cooling spikes also occur higher up
434 the profile where the drip water flows as a film along the speleothem surface (Figure 6).

435 Figure 7D-F contains the 2 weeks of winter monitoring that also coincide with the third
436 surface irrigation experiment 3. In winter (Figure 7D-F) the drip source shows regular daily
437 temperature fluctuations of ~0.8 ºC. Inspection of cave climate parameters reveals that the
438 cave air temperature fluctuates more and the RH less compared to summer (Figure 7E vs 7B).
439 Further, the outside air is almost continuously denser than the air in the shallow entrance area
440 (Figure 7F). Interestingly, the drip water temperature mainly reflected the pattern of the cave
441 air temperature while the drip rate (resulting from artificial surface irrigation during winter)
442 did not exceed ~25 drips in a 15 minute interval.

4. Discussion

Results presented in this paper allow, for the first time, a detailed identification of what controls the temperature of cave drip water. First we identify the controls and analyse how they affect drip water temperature, then we discuss their significance and implications in relation to interpreting speleothem records as paleoclimate archives.

4.1. What mechanisms control the cave drip water temperature?

Water movement to the drip source often occurs as film flow on cave deposits along variable distances [Dreybrodt et al., 2005; Camporeale and Ridolfi, 2012; Baker et al., 2014]. The data presented here demonstrates that cave drip water temperature is controlled by a number of simultaneous heat transport mechanisms that act upon the water film. Heat transfer between rock and water in karst conduits was analysed in detail by Covington et al. [2011], Covington et al. [2012] and Luhmann et al. [2015]. Dreybrodt et al. [2005] have theoretically analysed the heat and mass interactions involved in condensation corrosion involving water films. The engineering literature has recognised the complexity of film flow heat and mass exchange [i.e., Yan and Soong, 1995]. In relation to speleology our results are first in reporting and analysing heat transport processes that control cave drip water temperature.

The variety of different mechanisms and associated variables complicates quantification of the individual processes. Here, we focus on a detailed description of temperature characteristics that can be measured after water enters the cave and flows along cave features before arriving at the drip source. Figure 8 conceptualises the controls on drip water temperature. The individual heat transport mechanisms are discussed with reference to examples presented in the results.

Convective heat transport:

Heat convection due to subsurface water percolation ($q_{f,surf}$):

During the first surface irrigation experiment the water was deliberately cooled (Table 1) to test whether its thermal signature, transported by heat convection through the soil zone and the epikarst stores, is detectable at the drip source. The pre-existing large soil moisture deficit prior to surface irrigations was responsible for the first irrigation not producing any flow in the cave (Figure 5A). Due to the hot weather and general heat conduction towards the irrigated patch the cooled soil recovered to near normal temperatures between each of the cooled irrigations. While the second application was cold enough (~10 °C) for the thermal signature to be seen in the soil zone the cooling anomaly observed at the drip source

(locations k1 and k2 in Figure 5B) did not originate from the cooled surface irrigation. The main evidence for this conclusion is the lack of breakthrough of the deuterium enriched water (~6100 ‰ VSMOW) from the first irrigation (Figure 5C). The breakthrough of deuterium occurred after the third irrigation, indicating that the water travel time was significantly longer that the time between individual irrigations and the corresponding drip response in the cave. Markowska et al. [submitted] concluded that the water activating the drip came from epikarst stores. This also means that convection of cold water from the surface to the cave will take longer than the individual drip response time.

While the soil zone clearly responded to the three applications of cooled water at 2 separate locations (Figure 5A), the only signature attributable to the ice water detected at the drip source was a sharp short temperature fluctuation of only -0.8 °C on 10 Jan 2012 at 09:18 while the air temperature remained constant (blue arrow in Figure 5A). Importantly, this happened at a time during which fast film flow occurred over the flowstone, so this is not a temperature signal attributable to evaporative cooling (which only is dominant at slower flow). Interestingly, this short lasting cooling event was detected shortly after the start of the third surface irrigation (~35 mm rainfall equivalent) with ice-cooled water (~0 °C) while the soil was still cooled from the previous event. We interpret this as heat convection due to subsurface water percolation caused by fast preferential flow through the well wetted soil and fracture flow in the epikarst below. Note that first breakthrough of deuteriated water from the first surface irrigation was observed at the same time (Figure 5C and Markowska et al. [submitted]).

The above discussion illustrates that drip water temperature can be affected by thermal energy transported from the surface to the drip source through convection caused by subsurface water percolation. However, the prerequisites are that soil moisture is at field capacity, that preferential flow paths are still present and that the volume of water applied to the surface is much larger than the likely event based rainfall (105 mm was the maximum event based total between Oct 2011 and Dec 2014). In our case it took more than 133 mm rainfall equivalent (3 irrigations) of cooled water to produce a brief and small temperature anomaly. Furthermore, the experimental conditions were a worst case scenario in two other ways: 1) the temperature difference between the cooled irrigation water and the soil of 20-25 °C was unrealistically large for natural conditions, and 2) the section of the Cathedral Cave used in these experiments is very shallow with only about 1.7 m of soil and rock mass between the cave ceiling and the surface.

We expect that heat convection from subsurface water percolation caused by preferential flow through the soil and fracture flow through the epikarst can rarely cause drip water temperature anomalies that are significant for paleoclimate reconstructions from speleothems under realistic conditions. However, we acknowledge that this will depend on the thickness of the soil and epikarst as well as the fracture network above the cave. More research is needed to determine the conditions for which heat convection due to preferential or fracture flow from the surface can cause temperature anomalies that are of significance for speleothem-based paleoclimate reconstructions at drip sources.

Heat convection (q_f) due to film advection (v_f) along cave walls:

The mechanism of convective heat transport due to film advection is clearly illustrated in the drip water temperature response during surface irrigations 1 and 2 (see labelled areas in Figures 4A and 5B). Since it is summer, warmer water flows in films along the speleothem surfaces (v_f) where the thermal signature from above is carried with the water film (q_f) (Figures 4A and 5A). As a result of convective heat transport due to film advection the drip water temperature was raised by ~1 °C, but only at the start of the irrigation response (fastest drip rates on an event basis, here > 50 drips/min) and when a negative temperature-depth gradient existed (i.e., summer).

Temperature sensors located in the upper part of the profile (location b and c in Figure 2A) near the point at which water enters the cave detected a warmer water film compared to the surrounding air (Figure 4A). This thermal disequilibrium indicates heat convection due to fast preferential or fracture flow triggered by the surface irrigation [Cuthbert et al., 2014a]. However, it is important to note that the thermal energy causing the warming anomalies does not originate directly from the water applied to the surface. Instead, the anomalies originate from conduction between water film and rock higher up along the profile (explanation further below). Convective breakthrough between surface and cave only occurred under extreme circumstances, as pointed out in the previous subsection. The warming anomalies express a temporary downward shift of the localised conductive depth profile, i.e. they represent the temperature of the re-equilibration between the water film and the rock mass a short distance above the point of measurement. Here, we hypothesize that the magnitude of the convective signature is a function of the film advection rate (v_f proportional to the drip rate), the film thickness (b) and the flow distance (L). Baker et al. [2014] measured the thickness of water films on speleothems and found a dependency on the curvature and roughness of its surface.

Considering the number of unknowns and the fact that convective and conductive heat transport are both contributing during film flow, it is highly challenging to predict the water temperature as a function of distance.

As can be seen in the long-term drip water temperature record (Figure 6), film heat convection is initiated at the onset of drip events. However, it is most pronounced at the times with a large (exponential) temperature-depth gradient along the profile. This thermal gradient is caused by the conduction of the annual temperature signal into the subsurface rock mass. Consequently, the thermal effect of convection on drip water is a pronounced heating after summer and cooling after winter solstice. Further, it is most muted around the equinoxes due to a reversing temperature depth profile. Importantly, any convective influence on drip water temperature caused by film advection along cave walls will be muted at depths beyond the reach of the annual harmonic signal (see discussion further below).

Exchange of moisture (m_{atm}) and thermal energy ($q_{f,atm}$) between surface and cave:

When caves are open to the atmosphere air is exchanged [Conn, 1966], with the "chimney effect" (caused by an unstable density difference) being a common cause of venting [i.e., De Freitas et al., 1982; Oh and Kim, 2011]. Here we observe that the surface air is frequently denser than the shallow cave air during summer (Figure 7C) and continuously during winter (Figure 7F) which causes Cathedral Cave to be a well vented cave. At this point the question arises: How deep do venting events propagate into the cave?

Cuthbert et al. [2014] have shown that the drip water temperatures at a continuous slow drip source located ~40 m into the cave (site B) was continuously ~0.6 ºC cooler than the surrounding speleothem and air temperature, at a depth where conduction of heat from the surface is muted and where RH values are stable at ~92 %. Further, evaporation rates measured at different locations increasingly deeper in the cave show that the venting effect must dampen with distance from entry, which is consistent with observations in other caves [Perrier et al., 2010; Faimon et al., 2012]. However, despite the fact that the high frequency venting events do not directly show up at site C (Figure 1) a potential for evaporation does exist since the RH is ~97 %. Maintaining RH at less than saturation would not be possible without air exchange and, thus, drier and denser surface air must continuously replace moist and lighter air from deep within the cave.

Our findings are consistent with those from Buecher [1999] who reported a significant moisture loss at an average cave RH of 99.4 % due to venting in Kartchner Caverns located

572 in semi-arid Arizona. While cave venting has previously been investigated [Smithson, 1991;
573 Tarhule-Lips and Ford, 1998; Spotl et al., 2005] and its effects on the moisture loss have been
574 analysed [McLean, 1971; Buecher, 1999; De Freitas and Schmekal, 2003], we emphasize that
575 potentially significant amounts of thermal energy in the form of latent heat continuously
576 leaves the cave in the form of water vapour. This raises the question whether ongoing
577 evaporation and associated cooling can significantly lower the overall temperatures of caves
578 as well as individual drips? This could be answered by quantifying the energy lost through
579 latent heat as a fraction of the total cave energy balance.

580 **Conductive heat transport:**

581 Conduction of the surface temperature signal into the subsurface ($q_{c,atm}$):

582 Conduction of surface air temperature signals into the subsurface is a well-accepted
583 phenomenon [Smerdon et al., 2003, 2004]. Table 4 shows that the depth propagation of the
584 annual harmonic through rock mass complies well with the theory (Equation 1). Dominguez-
585 Villar et al. [2013] made use of cave thermal anomalies, measured in the cave air, to infer that
586 vegetation change at the surface influenced subsurface conduction. Further, the signature of
587 global warming was found in cave air temperature data at a depth of 37 m [Dominguez-Villar
588 et al., 2014]. We present 2 years of surface air temperature and cave air measurements, as
589 well as 1 year of speleothem, water film and drip water temperatures at different depths along
590 a flow profile. We illustrate that Equation 1 is able to predict the subsurface penetration of
591 the annual harmonic component by conduction from the ground surface temperature signal
592 considering multiple layers with different thermal properties. This should equally apply to
593 any other harmonic contained in the surface temperature signal as long as it is of sufficient
594 magnitude and duration not to be damped beyond detectability.

595 The data shown in Figures 3 and 6 demonstrate that the penetration of the annual temperature
596 variation controls the drip water temperature at site A. The surface temperature signal
597 generates the "background" temperature for drip water, but with exponentially damped
598 amplitude and linearly shifted phase proportional with depth. Here, the differences in mean
599 annual temperature can be explained with temperature changes that are slower than annual.

600 Conduction between speleothem and water film ($q_{c,rock}$):

601 The mechanism of heat conduction between speleothem and the water film, albeit "smeared"
602 by convection, is evident from the drip water temperatures measured during both irrigation

603 experiments (Figure 4A and Figure 5A). The first irrigation experiment (cooled water was
604 applied to the surface on three consecutive days, Figure 5) clearly illustrated that the pre-
605 existing temperature-depth gradient (the subsurface temperature decreases exponentially with
606 depth in summer) warmed the infiltrating colder irrigation water by conduction to produce
607 the arrival of warm pulses on the speleothem at the onset of dripping (Figure 5B). The time it
608 took for the deuteriated water to arrive at the drip source (Figure 5C) indicates a relatively
609 long residence time of water in the epikarst stores (~48 hours), for relatively large volumes of
610 water applied and an extreme temperature difference between water and rock. This
611 demonstrates that any temperature disequilibrium between rock and water from location b
612 onwards (Figure 2) must have originated from the subsurface rock mass. During irrigation
613 experiment 2 similar increases in the water temperature were observed after dripping had
614 started. Therefore, the increase in drip temperature after flow started was caused by
615 conduction from the warmer speleothem to the water further upstream of the profile
616 (exponentially decreasing rock temperature with depth in summer), followed by convective
617 heat transfer due to film advection, and subsequent conduction from the warmer water film
618 back into the rock further downstream [Cuthbert et al., 2014a].

619 The fact that the relative magnitude of the warming anomaly remained the same for sensors
620 located further along the profile is evidence for conduction between water film and rock
621 (Figure 4A). The amount of thermal energy conducted depends on the time that the water
622 film is in contact with a particular area of speleothem, the film thickness (b) and the
623 temperature difference. The contact time is determined by the velocity of the film flow (v_f),
624 which is proportional to the drip rate measured. There is a slow temperature tailing of the
625 water film and drip temperature (Figure 4A) in all records along the flow stone (L). This is
626 caused by conduction of thermal energy from the warmer water film back into the cooler
627 speleothem when convection becomes less significant than conduction at decreasing film
628 advection (= drip rates).

629 The temperature sensors that were inserted 4 cm into the speleothem confirm that the thermal
630 anomaly caused by the flowing water film is transferred into the speleothem. These sensors
631 show a temperature damping and lag with distance into the speleothem that is characteristic
632 of heat conduction (red lines in Figure 4A). Below a certain film advection rate (~20
633 drips/min in this case), convective warming ceases to dominate and is overwhelmed by
634 evaporative cooling (the cross-over of lines e & f in Figure 4A) illustrating that there is a
635 temporary thermal equilibrium (Figure 4A). Consequently, if the water film advection rate is

sufficiently slow or the film is thin enough the drip water temperature is controlled by the speleothem temperature but only in the absence of impacts from cave climate (i.e. evaporative cooling).

Conduction between air and water film or rock wall ($q_{c,air}$):

The cave air shows a vertical temperature gradient that is similar to the subsurface rock temperature gradient under stable conditions, i.e. no flow and no venting events (Figure 4A). Thermal anomalies can propagate much quicker through air than rock or water because the thermal diffusivity of air is approx. 22 and 146 times larger than that of the rock and water, respectively (Table 2). However, the heat capacity of air is in excess of ~4,000 and ~2,500 times smaller than water and rock, respectively. This means that the energy contained in thermal anomalies brought into the cave by air venting is effectively damped by the rock [Perrier et al., 2010]. Nevertheless, an example of heat conduction between air and drip water can be seen during irrigation experiment 1: A venting event transports cooler air from the atmosphere into the cave temporarily lowering the temperature of the drip source by ~1 °C (grey arrow in Figure 5A). The drip had ceased to be active at the time however the speleothem surface was still wet.

During winter the cave is continuously vented and the cave air temperature fluctuates periodically with varying amplitudes that depend on the surface climate (Figure 7E). This thermal signature is almost exactly replicated by the drip source temperature showing the mechanism of conduction between air and speleothem or air and water film (Figure 7D). The magnitude of temperature variation depends on the magnitude of airflow which is proportional to the air density difference [Faimon et al., 2012].

Latent heat and mass transport:

Latent heat ($q_{l,air}$) and mass (m_{air}) exchange between the water film and cave air:

Cuthbert et al. [2014a] previously demonstrated evaporative cooling of speleothem drip water, by as much as -1.5 °C compared to the cave air temperature. We have shown in new data presented here that this may be as high as -2.5 ºC (Figure 5). This anomaly was not caused by heat convection due to subsurface water percolation transporting the cooled irrigation water via preferential or fracture flow between surface and cave, as deuterium breakthrough had not yet occurred (Figure 5C). The cooling occurred because the previously dry flowstone surface was wetted by the drip response to surface irrigation. In fact, at one

location (k2 in Figure 5B) cooling of the wet flowstone to below air temperature continued after film flow had ceased. As the absence of dripping (and therefore film flow) rules out the possibility of convective cooling from cooled irrigation water applied to the surface, the cooling anomaly must be caused by evaporation.

In Figure 6 we present a new longer record of temperatures measured on 3 points along the speleothem surface including drip source (stalactite). It is obvious that frequent evaporative cooling events (Figure 7A) are directly coupled to venting events lowering the RH during summer (Figure 7C). Without venting the cave air RH would reach saturation over time and diminish the potential for evaporation. While Buecher [1999] found that cave evaporation rates are very sensitive to changes in RH, we observe that the vapour deficit also directly influences the magnitude of evaporative drip water cooling (Figures 4 and 7A-C).

From results presented here it is clear that air venting causes a complex thermodynamic coupling of cave and surface climate that influences the cave drip water temperature. We illustrate frequent and significant evaporative cooling and associated moisture exchange between drip water and cave air caused by frequent exchange of humid cave air with dry surface air. Dreybrodt et al. [2005] reported that cave walls can be warmed due to the release of latent heat during condensation in caves located in a humid climate. While our results show that in-cave evaporation can cause cooling, we anticipate that condensation could warm cave drip water. We illustrate that, when venting is present, cave drip water temperature near cave entrances can contain significant diurnal fluctuations or continuous cooling relative to cave air whenever RH is below a certain threshold. However, for drip water temperature to be affected by the cave climate it must be exposed to the cave air for some time before arriving at the drip source, e.g. as a water film flowing over speleothem surfaces such as flowstones, stalactites and draperies.

4.2. Implications for speleothem-based paleoclimate reconstructions

4.2.1. Relationship between temperature at the surface and drip source

Drip water temperature is a key variable to be considered when the paleoclimate records are reconstructed from speleothem archives. Current methods allow for paleo-temperature reconstruction (i.e. from $\delta^{18}O$) with seasonal and even monthly resolution [i.e., Treble et al., 2007; Orland et al., 2009]. The spatial resolution of speleothem milling, and therefore the temporal resolution of climate proxies, is likely to increase in the future with the development of better technologies. While the surface temperature is typically the result of interest, many

geochemical proxies depend on the temperature of the water at the drip source. This necessitates a better understanding of processes affecting the temperature at the surface of the speleothem at the time of its formation. Past surface climate estimates can be influenced by assumptions about the conditions along the flow path between surface and drip source.

Our results demonstrate that, in the absence of cave venting and convective thermal breakthrough from the surface, the drip water temperature is primarily a function of subsurface heat conduction, i.e. infiltrating surface water is quickly equilibrated to the subsurface temperature-depth profile. A universally applicable model to describe the relationship between surface and drip water temperature in this case is the differential equation for conductive heat transport [Carslaw and Jaeger, 1959]. It is important to note that thermal modelling requires subsurface thermal parameters such as presented in Table 2. However, these are in general reasonably well constrained and references to suitable literature can be found in Rau et al. [2014]. While significant temperature anomalies due to convective heat transport from the surface that could imprint on paleoclimate proxies can be ruled out in our case, we note that this could be possible under different karst settings. However, we expect the likeliness of such temperature anomalies to decreases with increasing subsurface depth.

The presence of the annual temperature signal in our data (Figure 3) facilitated the use of an analytical solution that is based on a harmonic temperature input at the surface (Equation 1). While this solution is useful for estimating the subsurface temperature response to cyclic drivers (e.g. annual, decadal, centennial or millennial), many paleoclimate events of interest are based on non-cyclic changes in the surface temperature, e.g. rapid climate change [Holmes et al., 2011]. Modelling the latter would require the selection of a suitable model to quantify the temperature evolution between surface and drip source. For example, the analytical solution used by Domínguez-Villar et al. [2013] describes the subsurface temperature as a function of depth and time based on a step change in surface temperature. Drip source temperature signals can be predicted from arbitrary surface temperature-time signals using a time convolution of this model. Vice versa, a deconvolution can unravel the surface temperature from a speleothem-based paleoclimate proxy.

4.2.2. Optimising the speleothem sampling location

Our measurements show that drip water temperature is controlled by a complex thermal coupling between the subsurface rock background temperature driven by the ground surface temperature and the cave climate driven by ventilation. This requires careful consideration

733 when deciding speleothem sampling locations. For example, the stalactite on which the drip
734 temperature was measured (Figure 2A-B) was exposed to an annual temperature variation of
735 ~5.21 °C as conducted from the surface but with a delay of ~2.6 months (80 days) compared
736 to the surface temperature signal. This is a significant variation when the temperature
737 dependency of speleothem growth is considered [Hendy, 1971; Casteel and Banner, 2014]
738 and if seasonal surface temperature is to be reconstructed.

739 Figure 9 shows the propagation of selected frequency components with an average soil zone
740 thickness of 0.1 m and an underlying epikarst to a depth of 100 m as a generic example but
741 also resembles the Cathedral Cave setting. Calculations are based on the laboratory
742 measurements of thermal parameters. Envelopes for minimum and maximum thermal
743 diffusivity for soil and bedrock as reported in the literature (Table 2) were also determined
744 for transferability of the results, i.e. when different materials are present at different field
745 sites. Figure 9 clearly illustrates the characteristic amplitude damping and phase shifting with
746 depth, inherent to the different harmonic signals. For example, it might be useful for a
747 researcher to maximise or minimise the annual temperature signal (which may determine the
748 presence of annual geochemical laminae useful for chronology building) compared to the
749 long-term paleoclimate signal. If a speleothem location was to be selected where the
750 maximum annual temperature variation should not be larger than 1 °C (0.5 °C amplitude) the
751 surface amplitude damping factor is ~0.059 (0.5 °C/8.51 °C). In the absence of venting and
752 convective heat transport through preferential or fracture flow, the desired variation is not
753 exceeded at total depths of greater than ~8.6 m (red dot in Figure 9A).

754 Another important consideration, when paleoclimate is to be inferred from speleothem
755 archives, is the phase shift. Again an example close to our case: A surface temperature signal
756 with centennial period is shifted by ~7.82 years (94 months) at 15 m depth (red dot in Figure
757 9B). Hence, this should be taken into account either when an accurate resolution of temporal
758 (i.e. seasonal) climate patterns is desired or when climatic patterns are compared to other
759 sources of information. Table 5 exemplifies minimum and maximum expected damping
760 factors and signal shifts for distinct depths extracted from Figure 9. This lag is within
761 resolution of long-record dating [Cheng et al., 2009] and could explain previous lag times
762 between drip source related signals and surface events [Domínguez-Villar et al., 2009].

763 The above discussion illustrates that the speleothem sampling location will not only depend
764 on the type of proxy (i.e., $\delta^{18}O$, $\delta^{13}C$, Δ_{47}, trace metals, organics) but also on what archived

765 harmonic signal resolution is desired. The increasing temporal resolution for drip source
766 temperature dependent proxies makes shallow sampling attractive to maximise the high
767 frequency temperature signal (i.e., seasonal to annual). However, near-entrance locations
768 require a good quantitative understanding on the influence from cave climate, such as
769 evaporation (or condensation) discussed below. Deep samples are better for long-term surface
770 dependent proxies as higher frequency temperature harmonics are essentially damped out.
771 Equations 1 and 2, as visualised in Figure 9 and Table 5, can serve as a guide for targeted
772 speleothem sampling.

773 **4.2.3. Cave venting and evaporation**

774 As a further point of discussion we illustrate that cave venting, besides influencing pCO_2
775 [Spotl et al., 2005; Baldini et al., 2008; Kowalczk and Froelich, 2010], can alter cave drip
776 water temperature and consequently influence speleothem growth. In fact, Casteel and
777 Banner [2014] illustrate that seasonal temperature variations control calcite growth rates and
778 trace element ratios. We emphasise that significant and frequent in-cave evaporation and drip
779 water cooling is to be expected for near-entrance parts of caves that are located in present (or
780 past) low humidity environments. Figure 10 summarises the evaporative cooling potential at
781 Cathedral Cave. While there is a weak correlation between drip water cooling and RH the
782 data exhibits significant scattering which indicates that additional parameters affect the
783 cooling, e.g. flow path, drip rate and air circulation. We observed up to -1.8 °C at a RH of <
784 95 % for drip water that is exposed to the cave air. Unravelling the dependency of drip water
785 evaporative cooling on venting clearly requires further research.

786 While we illustrate that evaporative drip water cooling is caused by regular ingress of dry air
787 during summer (Figure 7A-C), in-cave evaporation also occurs during winter as the outside
788 air is permanently denser (Figure 7D-F). Our results prove that Cathedral Cave is well vented
789 near the entrance despite the lack of discernible air movement. Results also indicate that
790 moisture escapes from even the deepest parts of the cave (RH < 100 %, evaporation rate > 0
791 mm) but measurable influences on the drip water temperature were not detected.

792 It is well accepted that venting influences geochemical signatures [Spotl et al., 2005; Baldini
793 et al., 2008]. We point out that evaporation leads to isotopic enrichment of drip water
794 [Cuthbert et al., 2014b; Markowska et al., submitted], and that evaporative drip water cooling
795 could significantly influence chemical/isotopic signatures in speleothems [Kim and O'Neil,
796 1997]. This may be a further complication in reconciling clumped isotope thermometry Δ_{47}

based temperature proxies in speleothems with mean air temperature, as Δ_{47} will be affected by the temperature of the water film from which the carbonate is precipitated [Affek et al., 2008].

Our results are consistent with Perrier et al. [2010] in that ventilation related effects, such as evaporation and associated cave rock and drip water temperature anomalies, are damped with increasing distance from the entrance. However, the magnitude of venting will strongly depend on the cave geomorphology [De Freitas et al., 1982]. In fact considerable air flow has been reported within caves [Conn, 1966; McLean, 1971; Cigna and Forti, 1986], in particular when multiple entries located at different vertical elevations are present [Faimon et al., 2012; Gregoric et al., 2013]. Figure 10 presents the first quantification of the effects of evaporative cooling of cave drip water. Our data is just from two drip sites in one cave, and further empirical field data is needed to develop a predictive model of factors determining the extent of evaporative cooling. However, the implications for speleothem temperature proxies are clear – in ventilated caves, researchers should consider the possibility that the speleothem proxy temperature is systematically cooler than the external mean air temperature.

4.2.4. Considerations for the type of speleothem to be sampled

A question arises as a result of the above discussion: What type of speleothem should be sampled to best constrain the drip water temperature? Site 1 has a stalagmite fed from a flowstone with a relatively long path (~3 m) where the water is exposed to the cave atmosphere via film flow. While we expect this type of speleothem would have a large potential for thermal disequilibrium affecting temperature proxies, it could still be a good source for soil or vegetation derived signals (i.e., pollen). A stalagmite fed by a regular conical-shaped stalactite will have drip water flowing along the outside of the deposit. This type of speleothem would be cooled during periods when the drip rate is slow and regular [Cuthbert et al., 2014a] which may imprint on the geochemical proxy and make interpretation difficult. We believe that the best stalagmite (likely a candlestick shape) for sampling is fed by a soda-straw stalactite because the flow path to the drip is surrounded by (thin) calcite and the water is therefore less exposed to the cave atmosphere and potential evaporative cooling. However, confirming this requires further research.

4.2.5. Summary

The implications of our results for speleothem paleoclimate reconstruction can be summarised as follows:

- The location that the proxy-derived temperature signal is representative for (i.e., surface or drip source) and the processes that could influence the signal must be carefully considered. Depending on the requirements, Equation 1 offers a quantitative model to convolve or deconvolve the "background" temperature signal between surface and drip source onto which in-cave signals will be superimposed.
- The damping of surface temperature variations in the soil/epikarst is a function of subsurface depth and frequency (Figure 9). If a surface temperature signal is required as a paleoclimate proxy (i.e., a decadal-scale temperature signal) a near-surface chamber, again with minimum venting and maximum relative humidity, should fulfil the conditions for sampling.
- Figure 9 illustrates the importance of considering the subsurface depth when speleothems are sampled for the purpose of accurately unravelling the surface temperature signal from isotope proxies. For example, highest amplitudes for the surface temperature during glacial-interglacial climate transitions and for the variability over the last 10,000 years are 5 °C and 0.5-1 °C, respectively [Cheng et al., 2009]. A rough guide for selecting appropriate sampling depths where the desired signal can be resolved is given in Table 5.
- We stress that, consistent with the results of Cuthbert et al. [2014a], frequent evaporative cooling events are to be expected in caves that could have been ventilated or exposed to evaporation (RH < 100 %). Evaporative cooling can lower the drip water temperature compared to cave air/speleothem temperature. The best cave locations to minimise this effect are those with a long-term RH of 100 % and no air flow. These criteria were set out in the 1960s to determine where to best sample speleothems for temperature records from ^{18}O [Hendy, 1971]. Here we show that, while the premise was correct, correction of the temperature signal should be considered. The influence could be assessed by checking for a difference in air and drip water temperature.
- The best speleothems to sample and analyse to obtain paleoclimate records of surface air temperature changes are minimum diameter stalagmites that are supplied by soda-straw stalactites. While the speleothem-water contact is maximised over water-air contact, the drip rates for these specimens are likely to be slow and evaporation could still occur, and therefore caves of RH of 100% and no air flow would provide ideal sampling locations.

5. Conclusion

Cave drip water temperature is controlled by multiple heat transfer mechanisms acting simultaneously during the movement of water through soil and bedrock and as film flow over speleothem surfaces, i.e. conduction, convection and latent heat and mass exchange. The two main heat sources/sinks are: 1) conduction of the dynamic surface temperature signal vertically into the subsurface, 2) the cave atmosphere as is coupled to the surface atmosphere by different venting mechanisms. The relative importance of each mechanism depends on the thickness of the overburden, the distance of film flow between entering the cave and the arriving at the drip source, and the advective velocity of the water film which is proportional to the drip rate.

While cave air temperatures have been measured and analysed in detail, there is a general lack of data and understanding relating to controls of cave drip water temperature. We deployed multiple specialised high-resolution sensors along an in-cave flow path and drip source to measure the evolution of the speleothem/water temperature. In-cave dripping was induced through manual surface irrigation experiments with cooled water and deuterium as a conservative tracer. In combination with measurements of drip rates, surface and cave climate, in-cave evaporation rates and deuterium concentrations we identified and analysed, for the first time, the heat transfer processes that exert control on the cave drip water temperature between surface and drip source.

Temperature harmonics contained in the surface temperature signal propagate conductively into the subsurface and undergo frequency dependent exponential amplitude damping and linear phase shifting with subsurface depth. For example, we observed that there is a clear exponential temperature-depth gradient induced by the annual surface temperature harmonic which controls the drip water temperature ("background" temperature). Film flow along the speleothem surface can convectively carry this signal down along the flow path causing temperature anomalies that depend on the film advection rate (which is proportional to the drip rate). However, this convective temperature anomaly is damped ("smeared") by conduction back into the speleothem along the flow path depending on the temperature-depth gradient at the time.

At the same time the water film is exposed to the cave air which can significantly change drip water temperature through convection/conduction or latent heat and mass exchange, with magnitudes that depend on the distance from the cave entrance. The influence on the water

temperature, however, depends on the film advection rate and the complex coupling between surface and cave climate through venting (i.e. air exchange induced by a density difference between surface and cave air). We observed regular evaporative drip water cooling events of -1.5 °C and up to -2.5 °C during summer when denser low-RH air enters the cave. Further, the drip water temperature can also fluctuate due to air-induced convection/conduction in winter when surface air is continuously denser (constant venting).

Drip water temperature is a key parameter controlling many biogeochemical in-cave processes that must be quantified when the paleoclimate is reconstructed from speleothem-based archives. We advise how the drip water "background" temperature can be modelled using simple analytical solutions of the differential heat conduction equation. We show how a data supported conceptual model for cave drip water temperature can assist with constraining a range of temperature sensitive biogeochemical speleothem processes. Further, we offer guidance on the type and location of speleothems that are sampled for paleoclimate signals with the intent to either maximise or minimise the drip water temperature signature. We anticipate that our findings will lead to significant improvements in the understanding of climate signals from speleothem based paleoclimate archives.

Acknowledgements

Funding for this research was provided by the National Centre for Groundwater Research and Training, an Australian Government initiative, supported by the Australian Research Council and the National Water Commission. Funding was also provided by the Gary Johnston fund that started the Chair of Water Management at UNSW. Mark Cuthbert was supported by Marie Curie Research Fellowship funding from the European Community's Seventh Framework Programme [FP7/2007-2013] under grant agreement n.299091. The climate station, Stalagmates and the specialised temperature monitoring equipment were provided by the Australian Government National Collaborative Research Infrastructure Strategy (NCRIS). We thank: Evan Jensen, Chris George, Col Birchall, Mike Augee and Eliza Wells for practical and logistical support during the irrigation experiments; Bruce Welsh and Philip Maynard from Sydney University Speleological Society for the cave survey map; Mark Whelan for help designing and building the high-resolution temperature equipment; Paul Brockbank from the School of Chemical Engineering workshop for his precision in drilling holes into a limestone sample so that thermal measurements could be conducted. The manuscript was significantly improved thanks to feedback from Claude Hillaire-Marcel (editor), Corrinne Wong (guest editor) and an anonymous reviewer.

References

Affek, H.P., Bar-Matthews, M., Ayalon, A., Matthews, A., Eiler, J.M., 2008. Glacial/interglacial temperature variations in Soreq cave speleothems as recorded by 'clumped isotope' thermometry. Geochimica et Cosmochimica Acta 72, 5351-5360, doi:http://dx.doi.org/10.1016/j.gca.2008.06.031.

Atkinson, T., Smart, P., Wigley, T., 1983. Climate and natural radon levels in Castleguard cave, Columbia Icefields, Alberta, Canada. Arctic and Alpine Research, 487-502

Baker, A., Genty, D., Dreybrodt, W., Barnes, W.L., Mockler, N.J., Grapes, J., 1998. Testing theoretically predicted stalagmite growth rate with recent annually laminated samples: Implications for past stalagmite deposition. Geochimica et Cosmochimica Acta 62, 393-404

Baker, A.J., Mattey, D.P., Baldini, J.U.L., 2014. Reconstructing modern stalagmite growth from cave monitoring, local meteorology, and experimental measurements of dripwater films. Earth and Planetary Science Letters 392, 239-249, doi:http://dx.doi.org/10.1016/j.epsl.2014.02.036.

Baker, D.G., Ruschy, D.L., 1993. The recent warming in eastern Minnesota shown by ground temperatures. Geophysical Research Letters 20, 371-374

Baldini, J.U., McDermott, F., Hoffmann, D.L., Richards, D.A., Clipson, N., 2008. Very high-frequency and seasonal cave atmosphere pCO2 variability: Implications for stalagmite growth and oxygen isotope-based paleoclimate records. Earth and Planetary Science Letters 272, 118-129

Bendjoudi, H., Cheviron, B., Guérin, R., Tabbagh, A., 2005. Determination of upward/downward groundwater fluxes using transient variations of soil profile temperature: test of the method with Voyons (Aube, France) experimental data. Hydrological processes 19, 3735-3745

BOM, 2014. Climate statistics for Australian locations: Wellington (Agrowplow). Bureau of Meteorology, Australian Government. http://www.bom.gov.au/climate/averages/tables/cw_065034_All.shtml, accessed: Dec 2014.

Buecher, R.H., 1999. Microclimate study of Kartchner caverns, Arizona. Journal of Cave and Karst Studies 61, 108-120.

Carslaw, H.S., Jaeger, J.C., 1959. Conduction of heat in solids, 2nd ed. Clarendon Press, Oxford.Camporeale, C., Ridolfi, L., 2012. Hydrodynamic-driven stability analysis of

955 morphological patterns on stalactites and implications for cave paleoflow reconstructions.
956 Physical review letters 108, 238501

957 Cheng, H., Edwards, R.L., Broecker, W.S., Denton, G.H., Kong, X., Wang, Y., Zhang, R.,
958 Wang, X., 2009. Ice Age Terminations. Science 326, 248-252, doi:10.1126/science.1177840.

959 Cheviron, B., Guérin, R., Tabbagh, A., Bendjoudi, H., 2005. Determining long-term effective
960 groundwater recharge by analyzing vertical soil temperature profiles at meteorological
961 stations. Water resources research 41

962 Clauser, C., Huenges, E., 1995. Thermal conductivity of rocks and minerals. Rock Physics
963 and Phase Relations: A Handbook of Physical Constants 3, 105-126,
964 doi:10.1029/RF003p0105.

965 Conn, H.W., 1966. Barometric wind in wind and jewel caves, South Dakota. The national
966 speleological society bulletin 28, 55-69

967 Covington, M.D., Luhmann, A.J., Gabrovšek, F., Saar, M.O., Wicks, C.M., 2011.
968 Mechanisms of heat exchange between water and rock in karst conduits. Water Resources
969 Research 47, W10514, doi:10.1029/2011WR010683.

970 Covington, M.D., Luhmann, A.J., Wicks, C.M., Saar, M.O., 2012. Process length scales and
971 longitudinal damping in karst conduits. Journal of Geophysical Research: Earth Surface 117,
972 F01025, doi:10.1029/2011JF002212.

973 Cuthbert, M.O., Baker, A., Jex, C.N., Graham, P.W., Treble, P.C., Andersen, M.S., Ian
974 Acworth, R., 2014b. Drip water isotopes in semi-arid karst: implications for speleothem
975 paleoclimatology. Earth and Planetary Science Letters 395, 194-204

976 Cuthbert, M.O., Rau, G.C., Andersen, M.S., Roshan, H., Rutlidge, H., Marjo, C.E.,
977 Markowska, M., Jex, C.N., Graham, P.W., Mariethoz, G., Acworth, R.I., Baker, A., 2014a.
978 Evaporative cooling of speleothem drip water. Scientific Reports 4, doi:10.1038/srep05162.

979 Davis, B.A.S., Brewer, S., Stevenson, A.C., Guiot, J., 2003. The temperature of Europe
980 during the Holocene reconstructed from pollen data. Quaternary Science Reviews 22, 1701-
981 1716, doi:http://dx.doi.org/10.1016/S0277-3791(03)00173-2.

982 De Freitas, C., Littlbjohn, R., Clarkson, T., Kristament, I., 1982. Cave climate: assessment of
983 airflow and ventilation. Journal of Climatology 2, 383-397

De Freitas, C., Littlejohn, R., 1987. Cave climate: assessment of heat and moisture exchange. Journal of Climatology 7, 553-569

De Freitas, C., Schmekal, A., 2003. Condensation as a microclimate process: measurement, numerical simulation and prediction in the Glowworm Cave, New Zealand. International Journal of Climatology 23, 557-575

De Vries, D.A., 1963. Thermal properties of soils. Physics of plant environment

Domínguez-Villar, D., Fairchild, I.J., Baker, A., Carrasco, R.M., Pedraza, J., 2013. Reconstruction of cave air temperature based on surface atmosphere temperature and vegetation changes: Implications for speleothem palaeoclimate records. Earth and Planetary Science Letters 369, 158-168

Domínguez-Villar, D., Fairchild, I.J., Baker, A., Wang, X., Edwards, R.L., Cheng, H., 2009. Oxygen isotope precipitation anomaly in the North Atlantic region during the 8.2 ka event. Geology 37, 1095-1098, doi:10.1130/g30393a.1.

Domínguez-Villar, D., Lojen, S., Krklec, K., Baker, A., Fairchild, I.J., 2014. Is global warming affecting cave temperatures? Experimental and model data from a paradigmatic case study. Climate Dynamics, 1-13

Dreybrodt, W., 1981. The kinetics of calcite precipitation from thin films of calcareous solutions and the growth of speleothems: revisited. Chemical Geology 32, 237-245

Dreybrodt, W., Gabrovšek, F., Perne, M., 2005. Condensation corrosion: a theoretical approach. Speleogenesis and Evolution of Karst Aquifers 3

Epstein, S., Buchsbaum, R., Lowenstam, H.A., Urey, H.C., 1953. Revised carbonate-water isotopic temperature scale. Geological Society of America Bulletin 64, 1315-1326

Faimon, J., Troppová, D., Baldík, V., Novotný, R., 2012. Air circulation and its impact on microclimatic variables in the Císařská Cave (Moravian Karst, Czech Republic). International Journal of Climatology 32, 599-623

Giacomo, P., 1982. Equation for the Determination of the Density of Moist Air (1981). Metrologia 18, 33

Hendy, C.H., 1971. The isotopic geochemistry of speleothems—I. The calculation of the effects of different modes of formation on the isotopic composition of speleothems and their

applicability as palaeoclimatic indicators. Geochimica et Cosmochimica Acta 35, 801-824, doi:http://dx.doi.org/10.1016/0016-7037(71)90127-X.

Holmes, J., Lowe, J., Wolff, E., Srokosz, M., 2011. Rapid climate change: lessons from the recent geological past. Global and Planetary Change 79, 157-162, doi:10.1016/j.gloplacha.2010.10.005.Horai, K.-i., 1971. Thermal Conductivity of Rock-Forming Minerals. Journal of Geophysical Research 76, 1278-1308, doi:10.1029/JB076i005p01278.

Jex, C.N., Mariethoz, G., Baker, A., Graham, P., Andersen, M.S., Acworth, I., Edwards, N., Azcurra, C., 2012. Spatially dense drip hydrological monitoring and infiltration behaviour at the Wellington Caves, South East Australia. International Journal of Speleology 41, 14

Kim, S.-T., O'Neil, J.R., 1997. Equilibrium and nonequilibrium oxygen isotope effects in synthetic carbonates. Geochimica et Cosmochimica Acta 61, 3461-3475, doi:http://dx.doi.org/10.1016/S0016-7037(97)00169-5.

Kowalczk, A.J., Froelich, P.N., 2010. Cave air ventilation and CO< sub> 2</sub> outgassing by radon-222 modeling: How fast do caves breathe? Earth and Planetary Science Letters 289, 209-219.

Luhmann, A.J., Covington, M.D., Myre, J.M., Perne, M., Jones, S.W., Alexander Jr, E.C., Saar, M.O., 2015. Thermal damping and retardation in karst conduits. Hydrol. Earth Syst. Sci. 19, 137-157, doi:10.5194/hess-19-137-2015.

Mariethoz, G., Baker, A., Sivakumar, B., Hartland, A., Graham, P., 2012. Chaos and irregularity in karst percolation. Geophysical Research Letters 39

Markowska, M., Baker, A., Andersen, M.S., Jex, C.N., Graham, P.W., Cuthbert, M.O., Rau, G.C., Rutlidge, H., Mariethoz, G., Marjo, C.E., Treble, P.C., Edwards, N., submitted. It's all about evaporation: artificial and natural water isotope tracing in semi-arid karst. Quaternary Science Reviews

McLean, J.S., 1971. The microclimate in Carlsbad Caverns, New Mexico. US Geological Survey, Albuquerque, New Mexico.

NIST, 2014. NIST Chemistry WebBook. National Institute of Standards and Technology, U.S. Department of Commerce. http://webbook.nist.gov/, accessed: Dec 2014.

Northup, E., Lavoie, K.H.D., 2001. Geomicrobiology of caves: a review. Geomicrobiology Journal 18, 199-222

1044 Ochsner, T.E., Horton, R., Ren, T., 2001. A New Perspective on Soil Thermal Properties.
1045 Soil Sci. Soc. Am. J. 65, 1641-1647, doi:10.2136/sssaj2001.1641.

1046 Oh, Y.H., Kim, G., 2011. Factors controlling the air ventilation of a limestone cave revealed
1047 by 222Rn and 220Rn tracers. Geosciences Journal 15, 115-119

1048 Orland, I.J., Bar-Matthews, M., Kita, N.T., Ayalon, A., Matthews, A., Valley, J.W., 2009.
1049 Climate deterioration in the Eastern Mediterranean as revealed by ion microprobe analysis of
1050 a speleothem that grew from 2.2 to 0.9 ka in Soreq Cave, Israel. Quaternary Research 71, 27-
1051 35, doi:http://dx.doi.org/10.1016/j.yqres.2008.08.005.

1052 Osborne, R., 2007. Cathedral Cave, Wellington Caves, New South Wales, Australia. A
1053 multiphase, non-fluvial cave. Earth Surface Processes and Landforms 32, 2075-2103

1054 Perrier, F., Le Mouël, J.-L., Richon, P., 2010. Spatial and Temporal Dependence of
1055 Temperature Variations Induced by Atmospheric Pressure Variations in Shallow
1056 Underground Cavities. Pure and applied geophysics 167, 253-276

1057 Rau, G.C., Andersen, M.S., McCallum, A.M., Roshan, H., Acworth, R.I., 2014. Heat as a
1058 tracer to quantify water flow in near-surface sediments. Earth-Science Reviews 129, 40-58

1059 Rutlidge, H., Baker, A., Marjo, C.E., Andersen, M.S., Graham, P.W., Cuthbert, M.O., Rau,
1060 G.C., Roshan, H., Markowska, M., Mariethoz, G., Jex, C.N., 2014. Dripwater organic matter
1061 and trace element geochemistry in a semi-arid karst environment: Implications for
1062 speleothem paleoclimatology. Geochimica et Cosmochimica Acta 135, 217-230,
1063 doi:10.1016/j.gca.2014.03.036.

1064 Schärli, U., Rybach, L., 2001. Determination of specific heat capacity on rock fragments.
1065 Geothermics 30, 93-110, doi:10.1016/S0375-6505(00)00035-3.

1066 Schön, J.H., 1996. Physical Properties of Rocks: Fundamentals and Principles of
1067 Petrophysics. 583

1068 Schouten, S., Woltering, M., Rijpstra, W.I.C., Sluijs, A., Brinkhuis, H., Sinninghe Damsté,
1069 J.S., 2007. The Paleocene–Eocene carbon isotope excursion in higher plant organic matter:
1070 Differential fractionation of angiosperms and conifers in the Arctic. Earth and Planetary
1071 Science Letters 258, 581-592

1072 Smerdon, J.E., Pollack, H.N., Cermak, V., Enz, J.W., Kresl, M., Safanda, J., Wehmiller, J.F.,
1073 2004. Air-ground temperature coupling and subsurface propagation of annual temperature
1074 signals. Journal of Geophysical Research: Atmospheres (1984–2012) 109

1075 Smerdon, J.E., Pollack, H.N., Enz, J.W., Lewis, M.J., 2003. Conduction-dominated heat
1076 transport of the annual temperature signal in soil. Journal of Geophysical Research: Solid
1077 Earth (1978–2012) 108

1078 Smithson, P., 1991. Inter-relationships between cave and outside air temperatures.
1079 Theoretical and applied climatology 44, 65-73

1080 Spötl, C., Fairchild, I.J., Tooth, A.F., 2005. Cave air control on dripwater geochemistry, Obir
1081 Caves (Austria): Implications for speleothem deposition in dynamically ventilated caves.
1082 Geochimica et Cosmochimica Acta 69, 2451-2468

1083 Tabbagh, A., Bendjoudi, H., Benderitter, Y., 1999. Determination of recharge in unsaturated
1084 soils using temperature monitoring. Water resources research 35, 2439-2446

1085 Tarhule-Lips, R.F., Ford, D.C., 1998. Condensation corrosion in caves on Cayman Brac and
1086 Isla de Mona. Journal of caves and karst studies 60, 84-95

1087 Tarnawski, V.R., Momose, T., Leong, W.H., 2011. Thermal Conductivity of Standard Sands
1088 II. Saturated Conditions. International Journal of Thermophysics 32, 984-1005,
1089 doi:10.1007/s10765-011-0975-1.

1090 Treble, P.C., Schmitt, A.K., Edwards, R.L., McKeegan, K.D., Harrison, T.M., Grove, M.,
1091 Cheng, H., Wang, Y.J., 2007. High resolution Secondary Ionisation Mass Spectrometry
1092 (SIMS) δ18O analyses of Hulu Cave speleothem at the time of Heinrich Event 1. Chemical
1093 Geology 238, 197-212, doi:http://dx.doi.org/10.1016/j.chemgeo.2006.11.009.

1094 Vosteen, H.-D., Schellschmidt, R., 2003. Influence of temperature on thermal conductivity,
1095 thermal capacity and thermal diffusivity for different types of rock. Physics and Chemistry of
1096 the Earth, Parts A/B/C 28, 499-509, doi:http://dx.doi.org/10.1016/S1474-7065(03)00069-X.

1097 Wigley, T., 1967. Non-steady flow through a porous medium and cave breathing. Journal of
1098 Geophysical Research 72, 3199-3205

1099 Yan, W.-M., Soong, C.-Y., 1995. Convective heat and mass transfer along an inclined heated
1100 plate with film evaporation. International Journal of Heat and Mass Transfer 38, 1261-1269,
1101 doi:http://dx.doi.org/10.1016/0017-9310(94)00241-M.

1102

Figure captions:

Figure 1: Survey map of Cathedral Cave located in the Wellington Caves Reserve in NSW, Australia. Instrumented sites are marked with red on the map.

Figure 2: A) Schematic subsurface cross-section of Site A (Figure 1) showing the drip water flow path along a flow stone to the stalactite (drip site) and the sensors deployed to measure water film and drip temperature and cave air temperature as well as climate parameters (humidity and pressure). B) A StarOddi micro T temperature sensor measuring at the drip source. C) Example of high-precision aluminium temperature sensor mounted on flow stone along the flow path (Australian 1-dollar coin with 25 mm diameter for scale).

Figure 3: Data from two years of monitoring at the Cathedral Cave: Surface air temperature, daily precipitation, and cave air temperature (measured at Site A1 Figure 1). For air temperatures, best fit to Equation 1 is indicated by dashed black lines. Blue lines are the drip water temperatures measured at Site A. Vertical dark grey bars show the times at which surface irrigation experiments were conducted coinciding with intense data collection periods. The light grey background indicates the times at which longer-term cave flowstone and drip water temperature was measured. The blue lines are speleothem and drip water temperature measurements enlarged in Figure 6 and explained later.

Figure 4: Drip monitoring with high time-resolution at site A during summer 2014. A) Temperature measured along a drip water flow path (for locations see Fig. 2a) on top of the flowstone (blue), at ~40 mm depth into the flowstone (red) and in the air (green). Surface air temperature is also plotted (grey). B) Drip rate and relative humidity. A total of 2 irrigations were conducted (vertical black lines indicating equivalent rainfall) with 3400 L and 2400 L applied to the surface irrigation patch. Parts of this data were previously published in Cuthbert et al. [2014a] to demonstrate evaporative cooling of speleothems. Light grey shaded areas indicate periods dominated by evaporative cooling. Dark grey shaded areas depict periods dominated by film convection.

Figure 5: Drip monitoring with high time-resolution at site A during summer 2013. A total of 4 irrigations were conducted with rainfall equivalents of 35 mm and 63 mm. A) Temperature measured at the tip of two neighbouring stalactites, and in the air (see Figure 2 for locations). Irrigations 1, 2 and 3 were cooled using bags with ice (irrigation water temperature is indicated next to the vertical black lines in a). B) Vertically enlarged temperature data from A. C) Deuterium measured in drip water samples during the irrigation experiment. Deuterium was added to the first irrigation (~6100 ‰ VSMOW). Min/max of the 2-year average from various drip sources at site A [Markowska et al., submitted]. D) Drip rate of both stalactites. The grey arrow (A and B) depicts the time when the surface air temperature was lower than the cave air temperature indicating cave venting. The blue arrow (B) shows the time at which the cooled surface irrigation caused a drip water temperature anomaly. Light grey shaded areas indicate periods of evaporative cooling. Dark grey shaded areas depict periods of film convection.

Figure 6: Temperatures measured at Site A on the flowstone surface where film flow occurred during times at which the drip source is active. Locations of the records are marked according to Figure 2. Data framed by grey vertical bars are highlighted in Figure 7. The highlighted winter dataset coincides with the surface irrigation experiment 3 (see also Figure 3).

Figure 7: Summer (A-C) and winter (D-F) snapshots of dry/wet speleothem and cave air temperature (A and D), cave climate (B and E), surface and cave air density (C and F). Note that the winter dataset (D-F) shows the response to surface irrigation experiment 3 (see Figure 3). Note that y-axes of subplot B, C, E and F have the same range for better signal comparison.

Figure 8: Conceptual model of the different controls on cave drip water temperature between surface and drip source. Individual heat and mass transfer mechanisms are depicted by arrows and described as follows: $q_{c,atm}$ is conduction between surface and subsurface, $q_{f,surf}$ is convection between surface and subsurface, $q_{f,atm}$ is convection between surface and cave air, m_{atm} is moisture exchange between surface and cave air, $q_{c,rock}$ is conduction between speleothem and water film, $q_{c,air}$ is conduction between water film and air, $q_{l,air}$ is latent heat

exchange between water film and air, m_{air} is moisture exchange between water film and air, q_f is convection of the water film, v_f is advection of the water film, L is the film flow distance between water entering the cave and drip source, b is the thickness of the water film.

Figure 9: Depth penetration of surface temperature components based on Equations 1-2 and thermal parameters in Table 2 with selected frequencies (daily, annual, decadal, centennial and millennial): A) amplitude damping, B) phase shift. The grey bands enveloping the curves reflect the variability arising from min/max thermal parameters reported in the literature. The red dots illustrate practical examples given in the discussion.

Figure 10: The evaporative cooling potential: Difference between cave air and drip water temperature plotted against RH. Site A: ~2 months of summer data (Figure 6). Site B: Data from the irrigation experiment 2 (Figure 3B in Cuthbert et al. [2014a]). Site C: ~4 months of measurements.

Table captions:

Table 1: Detailed summary of the individual surface irrigations conducted at 3 different times over a two year period between 2013 and 2014.

Table 2: Summary of thermal parameters of water, air, soil and limestone: [1]Water and air properties can be found in NIST [2014]. [2]Soil and limestone properties were measured in the laboratory using samples collected in the field. [3]Ranges for soil thermal parameters and limestone bedrock are from Ochsner et al. [2001] and Vosteen and Schellschmidt [2003].

Table 3: Cave evaporation rates measured at different locations and opposing seasons.

Table 4: Summary of results obtained by analysing temperature data from different locations with Equation 1 using an annual signal period ($P = 365.25$ days), soil zone thickness $d = 0.1$ m (except for surface air temperature), soil and limestone thermal diffusivity listed in Table 2. Phase offset is relative to summer solstice. The fitting algorithm minimised the NRMSE by varying the bold parameters.

Table 5: Max/min damping factors (ratio between subsurface and surface amplitude) and signal shifts for distinct depths and different harmonic signals extracted from Figure 9.

Tables

Date	Experiment / application	Water volume [litres]	Equiv. rain [mm]	Duration of irrigation [hours]	Equiv. rainfall intensity [mm/h]	Irrigation water temperature [ºC]
8/01/2013	1/1	840	~35	1.75	~20	0.3
9/01/2013	1/2	1500	~63	1.75	~35	10.6
10/01/2013	1/3	840	~35	1.75	~20	0.3
11/01/2013	1/4	1500	~63	1.75	~35	24.2
14/01/2014	2/1	3400	~68	2.85	~24	~25
15/01/2014	2/2	2400	~48	3.00	~16	~25
22/07/2014	3/1	1460	~29	1.00	~29	~12
23/07/2014	3/2	745	~15	0.50	~30	~12
24/07/2014	3/3	1460	~29	1.00	~29	~12

Table 1: Detailed summary of the individual surface irrigations conducted at 3 different times over a two year period between 2013 and 2014.

Material	Thermal conductivity [W/m/K]	Specific heat capacity [MJ/m^3/K]	Thermal diffusivity [m^2/d]	Min. thermal diffusivity [m^2/d]	Max. thermal diffusivity [m^2/d]
Water @ 18 °C	0.595[1]	4.180[1]	0.0123[1]	-	-
Air @ 18 °C	0.025[1]	0.001[1]	1.8014[1]	-	-
Soil (dry)	0.545[2]	1.188[2]	0.0396[2]	-	-
Soil (saturated)	0.835[2]	2.939[2]	0.0245[2]	-	-
Soil	-	-	0.03[3]	0.01[3]	0.06[3]
Limestone	2.356[2]	2.518[2]	0.0808[2]	0.06[3]	0.14[3]

Table 2: Summary of thermal parameters of water, air, soil and limestone: [1]Water and air properties can be found in NIST [2014]. [2]Soil and limestone properties were measured in the laboratory using samples collected in the field. [3]Ranges for soil thermal parameters and limestone bedrock are from Ochsner et al. [2001] and Vosteen and Schellschmidt [2003].

Evaporation rate [mm/year]		
Location	Summer (January 2014)	Winter (July 2014)
Near entrance	440	
Site A	50	>56
Site B	40	
Site C	13	4.8

Table 3: Cave evaporation rates measured at different locations and opposing seasons.

Temperature measurement location	**Mean**	**Amplitude**	**Phase**	**Phase offset**	**Total depth**	**NRMSE**	**Number of data points**
Parameter [unit]	T_0 [ºC]	A [ºC]	[d]	θ [d]	z [m]	[-]	[-]
Surface air	**16.90**	**8.51**	0	**20.0**	0	0.1827	52,376
Flowstone (b, Site A)	**17.18**	5.03	30.7	**31.9**	**1.55**	0.2579	30,810
Flowstone (c, Site A)	**16.62**	4.11	42.4	**31.8**	**2.16**	0.2341	30,811
Stalactite (j, Site A)	**16.11**	2.61	68.8	**31.2**	**3.55**	0.1653	30,814
Cave air (Site A)	**16.32**	2.38	74.1	**31.4**	**3.83**	0.3609	23,750
Cave air (Site A1)	**15.70**	1.65	95.6	**31.1**	**4.95**	0.3400	29,338
Cave air (Site C)	18.10	-	-	-	~25	-	17,959

Table 4: Summary of results obtained by analysing temperature data from different locations with Equation 1 using an annual signal period ($P = 365.25$ days), soil zone thickness $d = 0.1$ m (except for surface air temperature), soil and limestone thermal diffusivity listed in Table 2. Phase offset is relative to summer solstice. The fitting algorithm minimised the NRMSE by varying the bold parameters.

Harmonic		daily		annual		decadal		centennial		millennial	
Depth [m]		**Min**	**Max**	**Min**	**Max**	**Min**	**Max**	**Min**	**Max**	**Min**	**Max**
0.1	Amp [-]	0.17	0.49	0.91	0.96	0.97	0.99	0.99	1.00	1.00	1.00
	Phase [months]	0.0	0.0	0.1	0.1	0.3	0.4	0.9	1.3	2.8	4.0
1	Amp [-]	0	0.01	0.65	0.77	0.87	0.92	0.96	0.97	0.99	1.00
	Phase [months]	-	0	0.5	0.8	1.6	2.5	5.1	7.8	16.3	24.5
10	Amp [-]	0	0	0.02	0.08	0.30	0.46	0.68	0.78	0.89	0.92
	Phase [months]	-	-	4.8	7.3	15.1	23.0	47.8	72.8	151.0	230.3
100	Amp [-]	0	0	0	0	0	0	0.02	0.08	0.30	0.46
	Phase [months]	-	-	-	-	-	-	473	723	1498	2288

Table 5: Max/min damping factors (ratio between subsurface and surface amplitude) and signal shifts for distinct depths and different harmonic signals extracted from Figure 9.

Figure 1

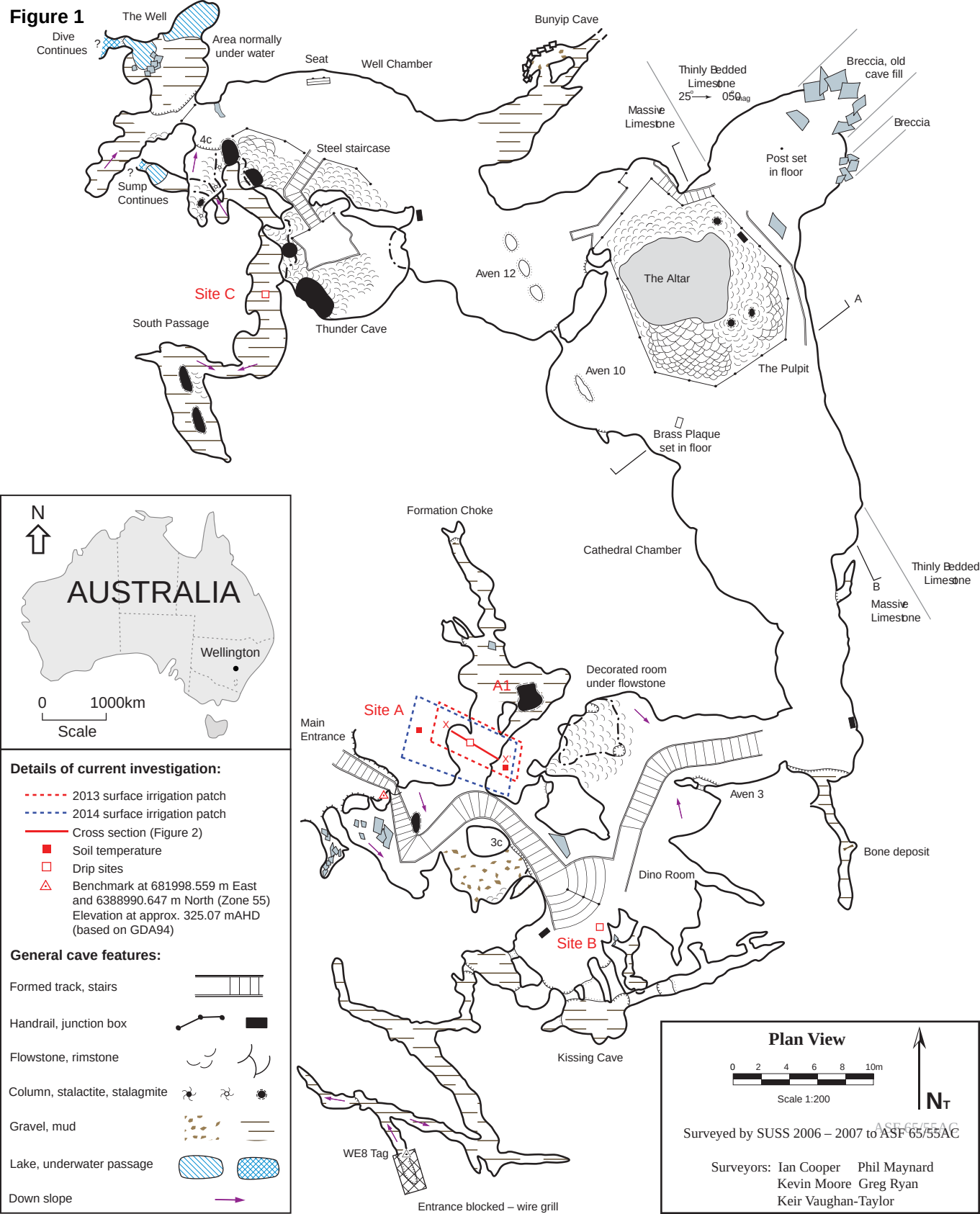

Details of current investigation:

- 2013 surface irrigation patch
- 2014 surface irrigation patch
- Cross section (Figure 2)
- Soil temperature
- Drip sites
- Benchmark at 681998.559 m East and 6388990.647 m North (Zone 55) Elevation at approx. 325.07 mAHD (based on GDA94)

General cave features:

- Formed track, stairs
- Handrail, junction box
- Flowstone, rimstone
- Column, stalactite, stalagmite
- Gravel, mud
- Lake, underwater passage
- Down slope

Plan View

0 2 4 6 8 10m

Scale 1:200

N_T

Surveyed by SUSS 2006 – 2007 to ASF 65/55AC

ASF 65/55AC

Surveyors: Ian Cooper Phil Maynard
Kevin Moore Greg Ryan
Keir Vaughan-Taylor

Figure 2 Surface irrigation area (Figure 1)

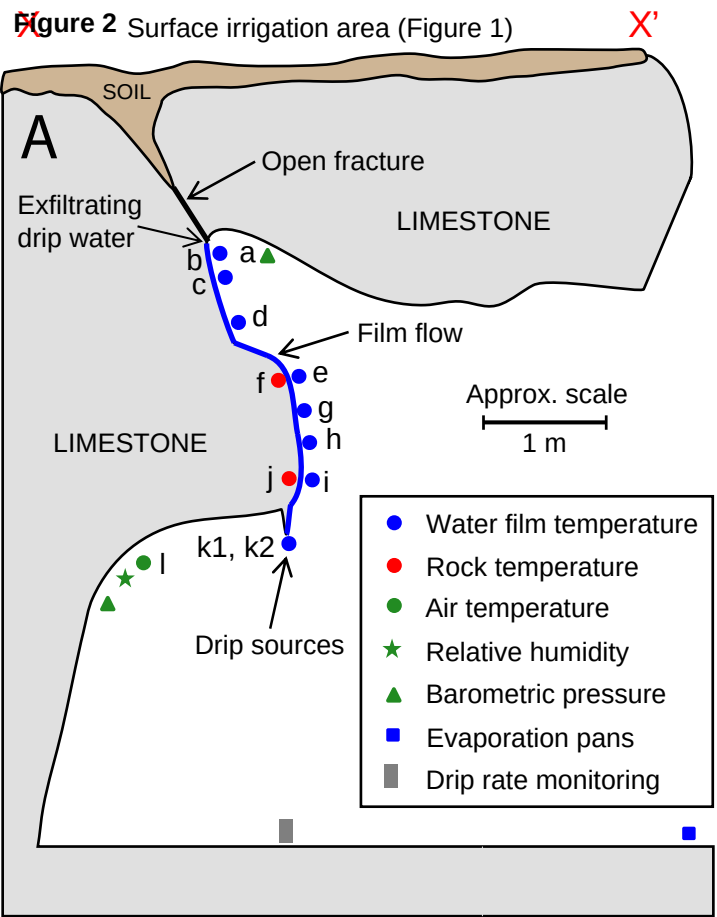

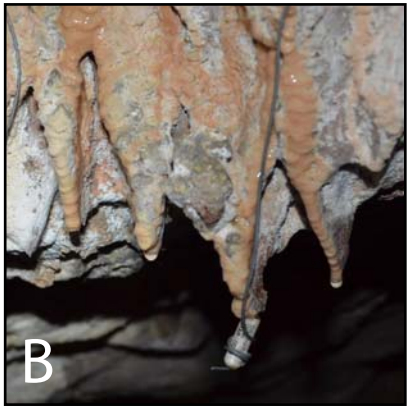

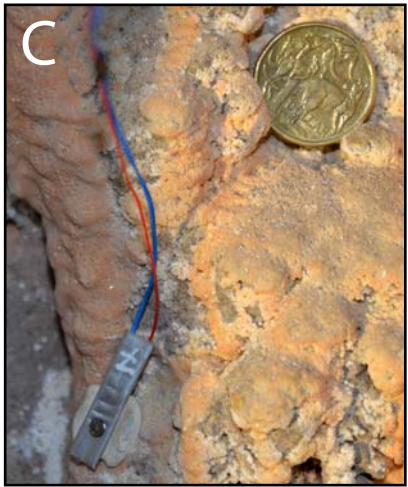

Figure 3

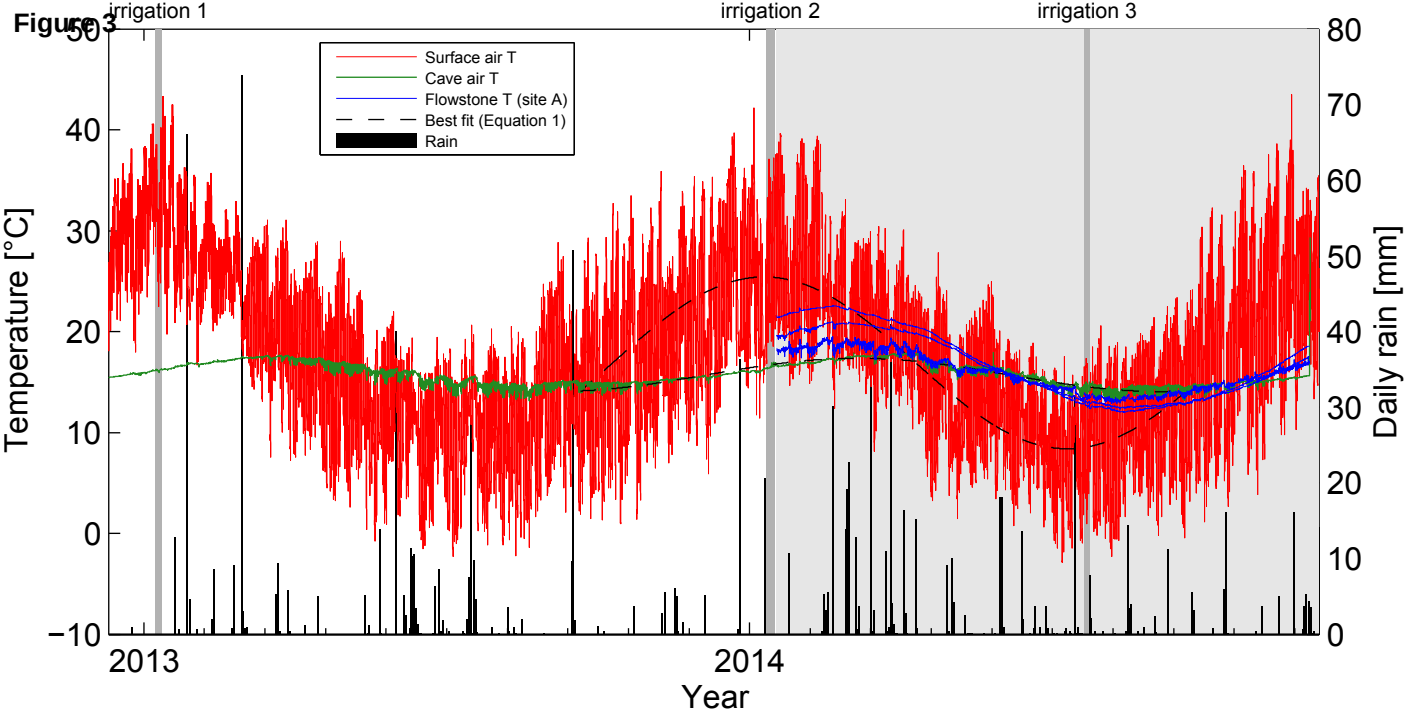
irrigation 1
irrigation 2
irrigation 3
Surface air T
Cave air T
Flowstone T (site A)
Best fit (Equation 1)
Rain
Temperature [°C]
Daily rain [mm]
Year
2013
2014
50
40
30
20
10
0
−10
80
70
60
50
40
30
20
10
0

Figure 4

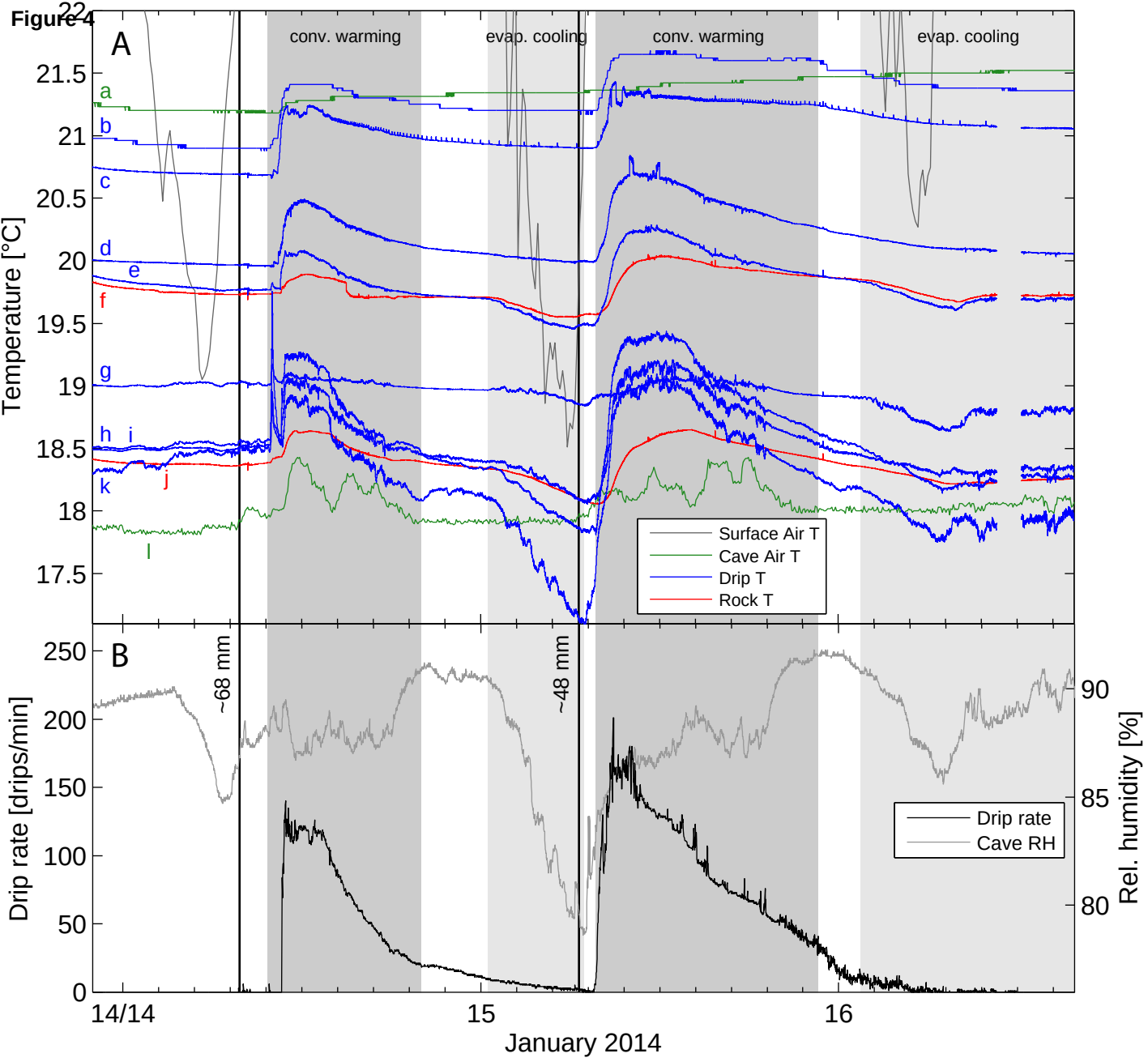
A
conv. warming
evap. cooling
conv. warming
evap. cooling
Temperature [°C]
22
21.5
21
20.5
20
19.5
19
18.5
18
17.5
a
b
c
d
e
f
g
h
i
j
k
l
Surface Air T
Cave Air T
Drip T
Rock T
B
~68 mm
~48 mm
Drip rate [drips/min]
250
200
150
100
50
0
90
85
80
Rel. humidity [%]
Drip rate
Cave RH
14/14
15
16
January 2014

Figure 5

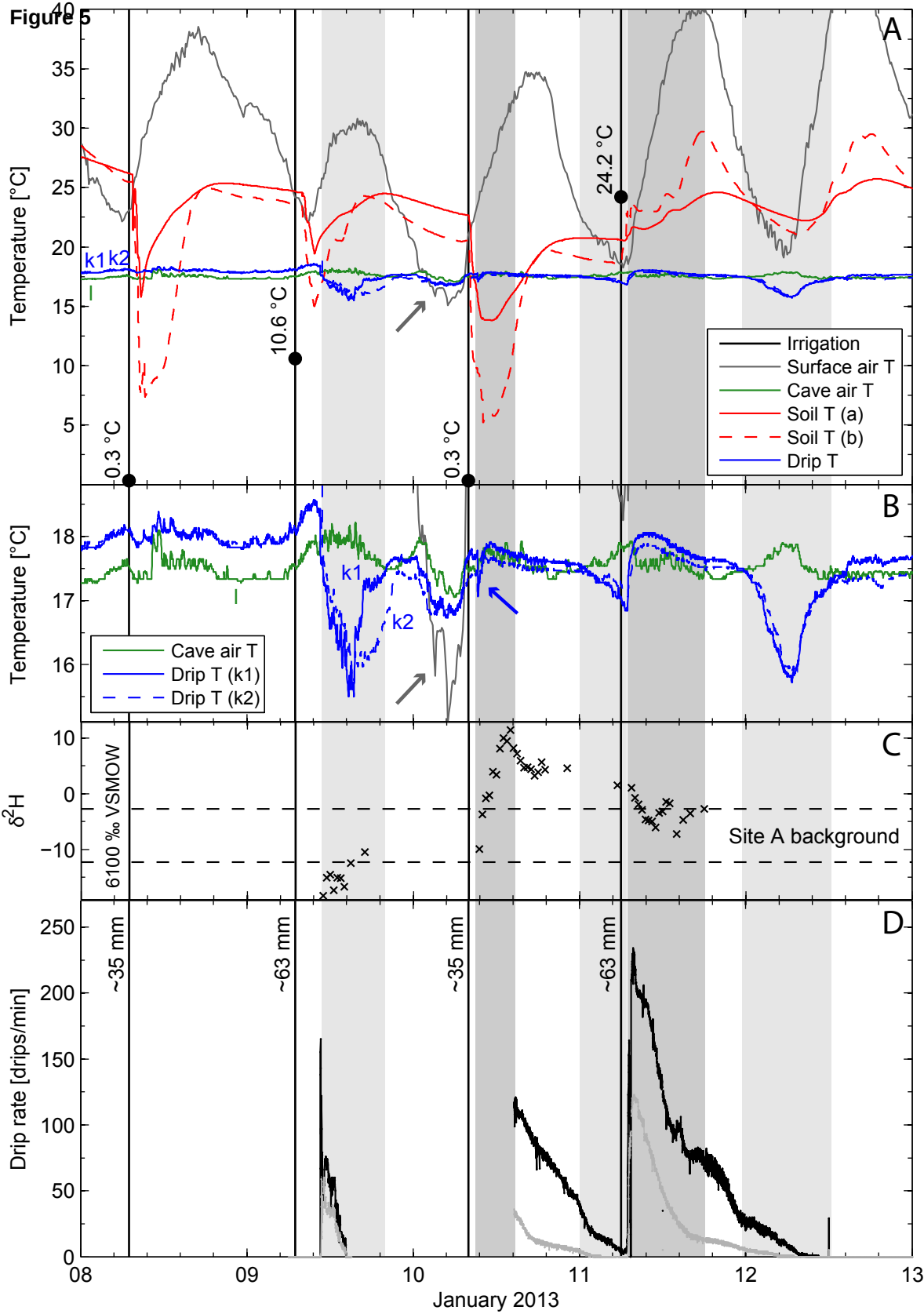
A
Temperature [°C]
Irrigation
Surface air T
Cave air T
Soil T (a)
Soil T (b)
Drip T
k1 k2
I
0.3 °C
10.6 °C
0.3 °C
24.2 °C
B
Temperature [°C]
Cave air T
Drip T (k1)
Drip T (k2)
k1
k2
I
C
δ2H
6100 ‰ VSMOW
Site A background
D
Drip rate [drips/min]
~35 mm
~63 mm
~35 mm
~63 mm
08
09
10
11
12
13
January 2013

Figure 6

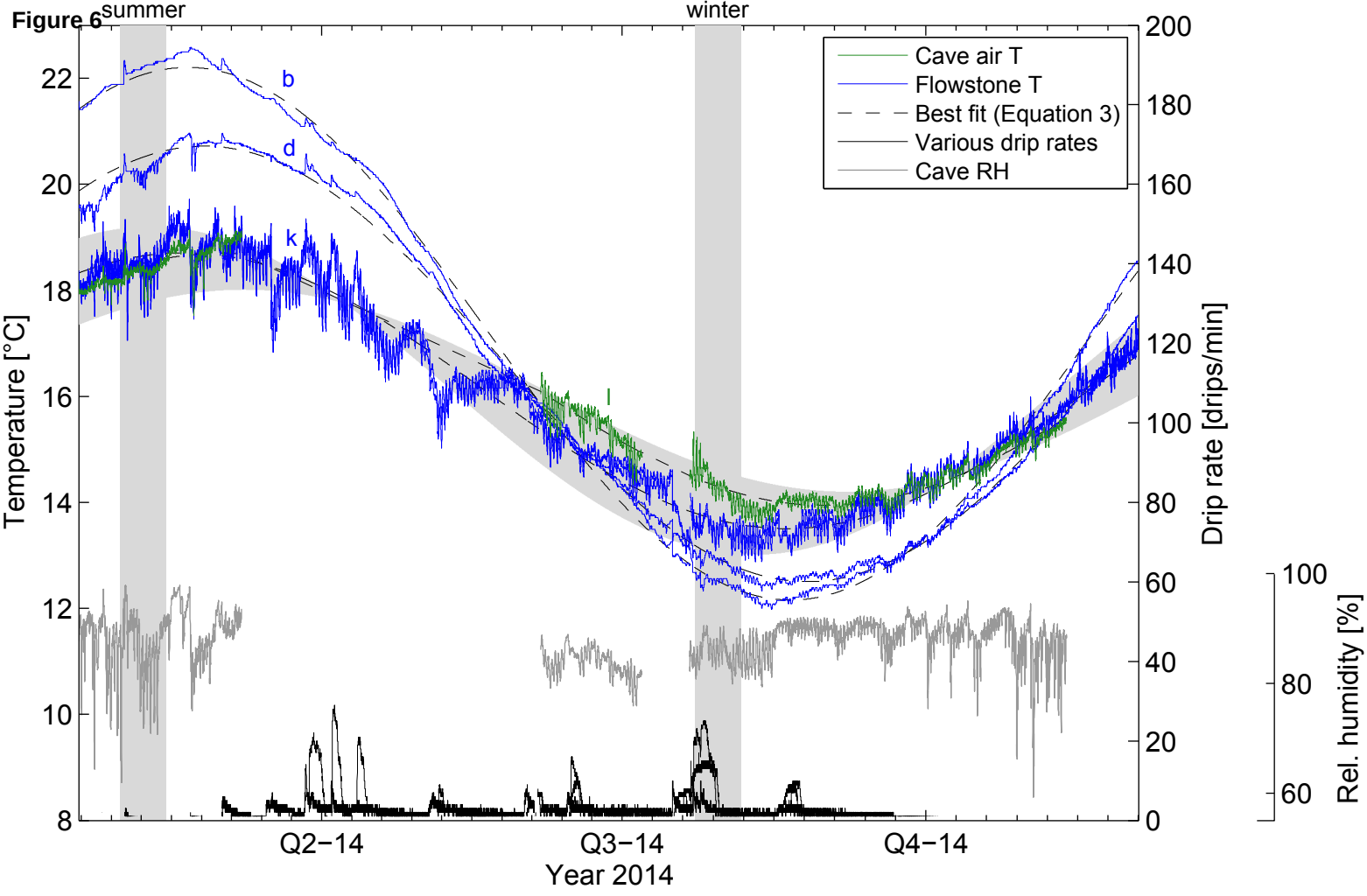
summer
winter
b
d
k
l
Cave air T
Flowstone T
Best fit (Equation 3)
Various drip rates
Cave RH
Temperature [°C]
Drip rate [drips/min]
Rel. humidity [%]
Q2−14
Q3−14
Q4−14
Year 2014

Figure 7

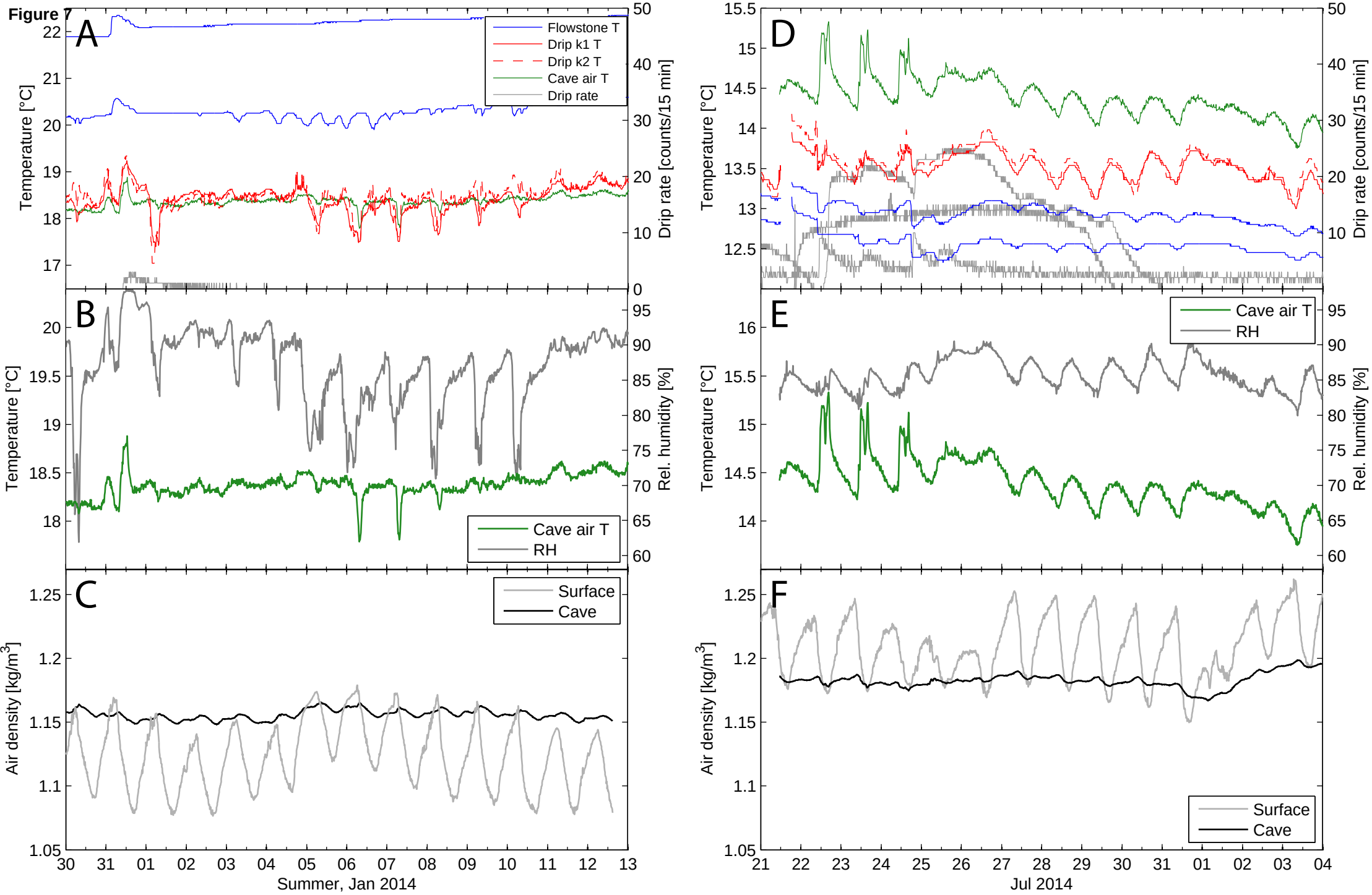
A
Flowstone T
Drip k1 T
Drip k2 T
Cave air T
Drip rate
Temperature [°C]
Drip rate [counts/15 min]
B
Cave air T
RH
Temperature [°C]
Rel. humidity [%]
C
Surface
Cave
Air density [kg/m3]
Summer, Jan 2014
D
Temperature [°C]
Drip rate [counts/15 min]
E
Cave air T
RH
Temperature [°C]
Rel. humidity [%]
F
Surface
Cave
Air density [kg/m3]
Jul 2014

Figure 8

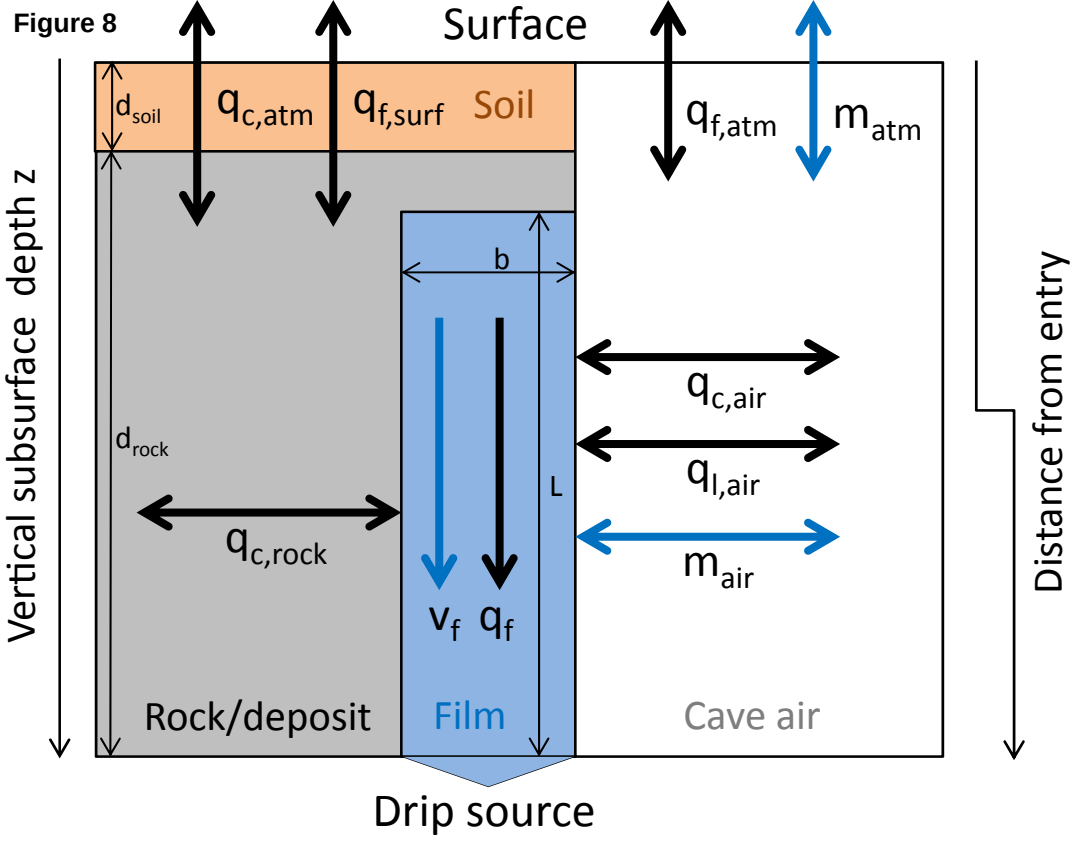
Surface
d_{soil}
$q_{c,atm}$
$q_{f,surf}$
Soil
$q_{f,atm}$
m_{atm}
b
$q_{c,air}$
$q_{l,air}$
m_{air}
d_{rock}
L
$q_{c,rock}$
v_f q_f
Vertical subsurface depth z
Distance from entry
Rock/deposit
Film
Cave air
Drip source

Figure 9

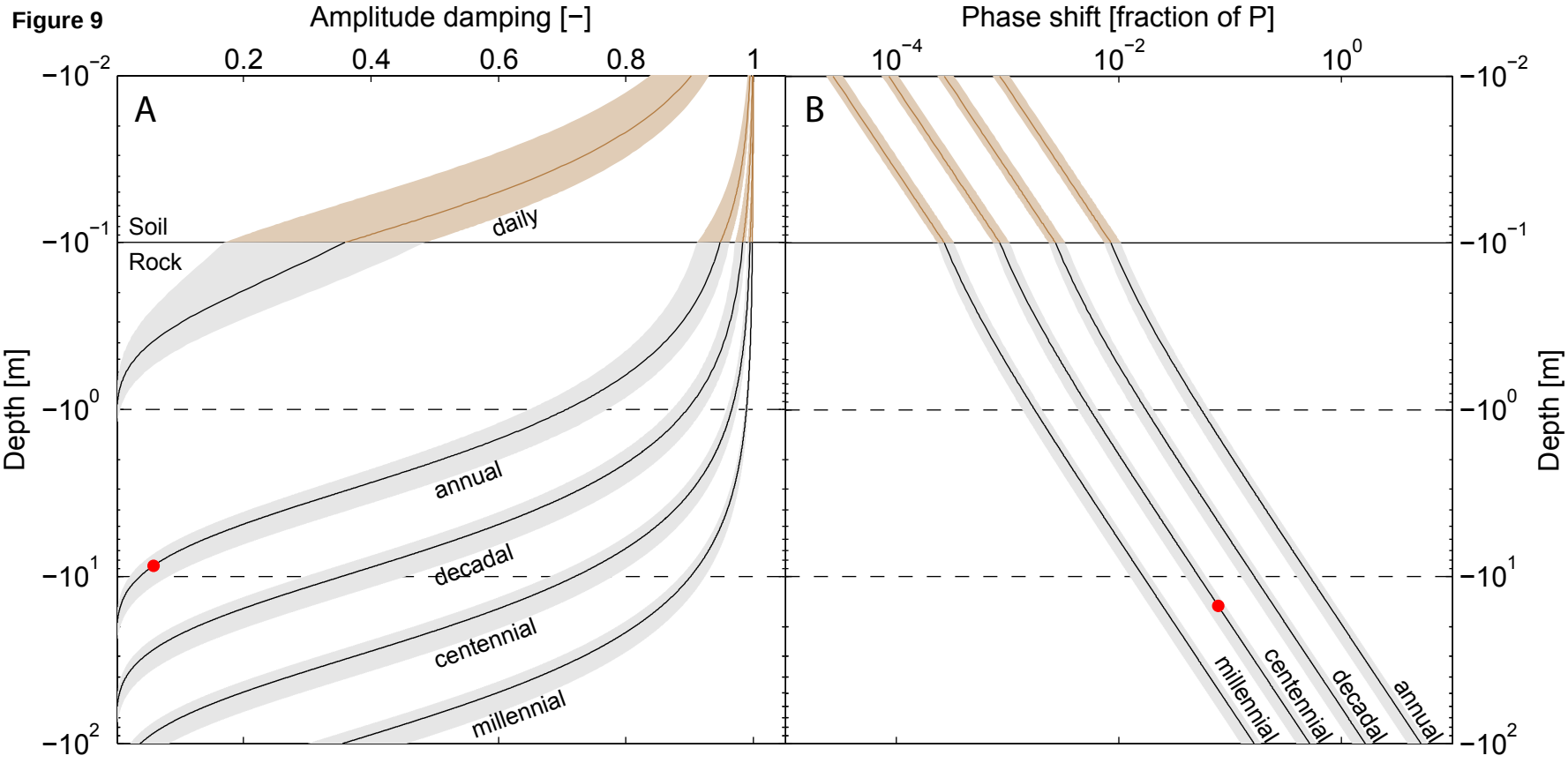
Amplitude damping [−]
0.2
0.4
0.6
0.8
1
Phase shift [fraction of P]
10^{-4}
10^{-2}
10^{0}
A
B
Soil
Rock
daily
annual
decadal
centennial
millennial
-10^{-2}
-10^{-1}
-10^{0}
-10^{1}
-10^{2}
Depth [m]

Figure 10

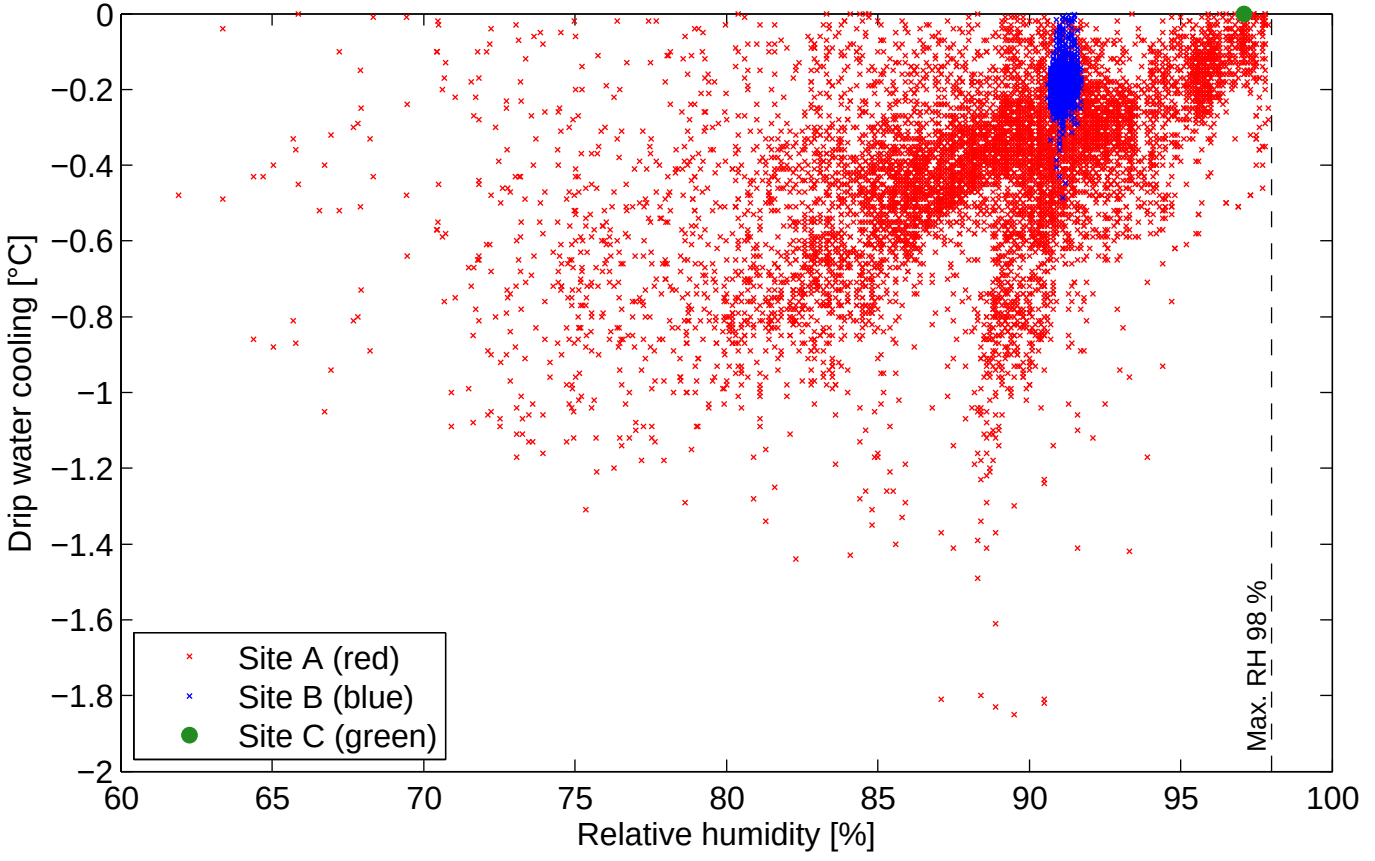
0
−0.2
−0.4
−0.6
−0.8
−1
−1.2
−1.4
−1.6
−1.8
−2
Drip water cooling [°C]
60
65
70
75
80
85
90
95
100
Relative humidity [%]
Site A (red)
Site B (blue)
Site C (green)
Max. RH 98 %